JCB

Article

Srf controls satellite cell fusion through the maintenance of actin architecture

Voahangy Randrianarison-Huetz,[1,2,3]* Aikaterini Papaefthymiou,[1,2,3]* Gaëlle Herledan,[1,2,3] Chiara Noviello,[1,2,3] Ulduz Faradova,[1,2,3] Laura Collard,[4] Alessandra Pincini,[1,2,3] Emilie Schol,[1,2,3] Jean François Decaux,[5] Pascal Maire,[1,2,3] Stéphane Vassilopoulos,[6] and Athanassia Sotiropoulos[1,2,3]

[1]Institut National de la Santé et de la Recherche Médicale U1016, Institut Cochin, Paris, France
[2]Centre National de la Recherche Scientifique UMR8104 and [3]Université Paris Descartes, Paris, France
[4]Francis Crick Institute, London, England, UK
[5]Université Pierre et Marie Curie Paris 6, Centre National de la Recherche Scientifique UMR8256, Institut National de la Santé et de la Recherche Médicale U1164, Institute of Biology Paris-Seine, Paris, France
[6]Institut National de la Santé et de la Recherche Médicale/University Pierre and Marie Curie UMR-S974, Institut de Myologie, Paris, France

Satellite cells (SCs) are adult muscle stem cells that are mobilized when muscle homeostasis is perturbed. Here, we show that serum response factor (Srf) is needed for optimal SC-mediated hypertrophic growth. We identified Srf as a master regulator of SC fusion required in both fusion partners, whereas it was dispensable for SC proliferation and differentiation. We show that SC-specific Srf deletion leads to impaired actin cytoskeleton and report the existence of finger-like actin–based protrusions at fusion sites in vertebrates that were notoriously absent in fusion-defective myoblasts lacking Srf. Restoration of a polymerized actin network by overexpression of an α-actin isoform in Srf mutant SCs rescued their fusion with a control cell in vitro and in vivo and reestablished overload-induced muscle growth. These findings demonstrate the importance of Srf in controlling the organization of actin cytoskeleton and actin-based protrusions for myoblast fusion in mammals and its requirement to achieve efficient hypertrophic myofiber growth.

Introduction

Adult skeletal muscle possesses a tremendous degree of plasticity, as it can adapt its size to various stresses such as functional overload, and can efficiently regenerate after injury. Skeletal muscle tissue contains multinucleated postmitotic myofibers and a small resident muscle stem cell population, known as satellite cells (SCs). In undamaged muscle, SCs are maintained in a quiescent state and express the transcription factor Pax7. In response to muscle lesion or increased load, activated cells divide to form a pool of proliferating myoblasts (MBs) that coexpress Pax7, Myf5, and MyoD. Cells committed to myogenic lineage progression and differentiation exit the cell cycle, decrease expression of Pax7, and express MyoD and Myogenin. Most SCs progress along the myogenic lineage and fuse to form new myofibers (during regeneration) or supplement existing growing muscle fibers (during hypertrophy), and a subset of SCs maintain Pax7 expression and revert back to quiescence to replenish the SC pool (Dumont et al., 2015; Almada and Wagers, 2016). Thus, both repair and growth of multinucleated skeletal muscle cells are dependent on the fusion of muscle progenitor cells.

The fusion process follows an ordered set of cellular events that includes cell migration, alignment, adhesion, and membrane fusion. Many molecules, including secreted factors, membrane receptors, and intracellular molecules, participate in MB fusion (Hindi et al., 2013). In *Drosophila melanogaster*, fusion is accompanied by extensive rearrangement of the actin cytoskeleton, at the site of MB contact, highlighted by the formation of an actin-based invasive podosome-like protrusion structure (Sens et al., 2010; Kim et al., 2015a; Martin, 2016; Schejter, 2016), which in turn may provide the necessary pushing force to bring plasma membranes in close apposition for fusion to occur (Kim et al., 2015b). In addition, actin-based filopodia were shown to facilitate MB and myotube (MT) recognition/adhesion before MB fusion in adult *Drosophila* myogenesis (Segal et al., 2016). The essential role of the actin cytoskeleton in fusion is conserved in mammals, in which the actin regulators Rac1, Cdc42, and N-Wasp are required for the fusion process during muscle development (Vasyutina et al., 2009; Gruenbaum-Cohen et al., 2012). However, there is no evidence for discrete actin-based structures associated with the fusion process in vertebrates during muscle development, adult muscle regeneration, or hypertrophy or in primary muscle cell cultures.

Serum response factor (Srf) transcription factor controls the expression of target genes involved in cell growth, migration, and cytoskeletal organization (Esnault et al., 2014). Among Srf

*V. Randrianarison-Huetz and A. Papaefthymiou contributed equally to this paper.
Correspondence to Athanassia Sotiropoulos: athanassia.sotiropoulos@inserm.fr

The Rockefeller University Press
J. Cell Biol. Vol. 217 No. 2 685–700
https://doi.org/10.1083/jcb.201705130

targets, some are specifically expressed in skeletal muscle, including *MyoD* and several genes encoding sarcomeric proteins (*α-actins* and *myosin light chain*; Pipes et al., 2006). The ability of Srf to regulate transcription depends on its association with cofactors (Posern and Treisman, 2006; Gualdrini et al., 2016), such as the Myocardin-related transcription factors (MrtfA and MrtfB). The Rho family of small GTPases and actin dynamics have been shown to control the nuclear accumulation of Mrtf-A/B and therefore modulate Srf activity (Posern and Treisman, 2006; Nordheim, 2014). Thus, the actin/Mrtf/Srf pathway forms a conserved homeostatic feedback system to ensure that actin levels are appropriate to support the actin dynamics required for complex cell behavior by controlling the expression of numerous genes involved in actin cytoskeletal structures and treadmilling, while being regulated itself by actin dynamics (Esnault et al., 2014; Kalo et al., 2015).

In mammals, the deletion of Srf in muscle progenitors during embryonic development impairs muscle formation (Li et al., 2005). Experiments performed using the C2C12 muscle cell line have shown that functional Srf is required for MyoD expression, MB proliferation, and differentiation (Gauthier-Rouviere et al., 1996; Soulez et al., 1996; Carnac et al., 1998). The use of mouse genetic models with the specific loss of *Srf* in myofibers showed that Srf is required for postnatal and adult muscle growth in vivo (Li et al., 2005; Charvet et al., 2006; Guerci et al., 2012) and that the decrease of Srf activity plays a functional role in disuse muscle atrophy (Collard et al., 2014). However, there are no data on the role played by Srf in SC behavior in vivo during adult muscle remodeling. Srf activity may be required to control SC cell fate in vivo in various situations of stress by controlling genes involved in cell proliferation (immediate early genes), myogenic differentiation (*MyoD*, *α actins*, and *myosins*), and actin architecture.

Here, we assessed the role played by Srf in SCs under stress conditions by inducing compensatory hypertrophy (CH) of plantaris muscles harboring a conditional and inducible deletion of Srf in the SCs and showed compromised hypertrophic muscle growth in the absence of Srf. We showed that Srf in SCs is not essential for *MyoD* expression, SC proliferation, or differentiation, in contrast to what was reported in the C2C12 cell line. However, the motility and fusion capacities of SCs lacking *Srf* were blunted and were accompanied by impaired actin cytoskeleton. Both homotypic (between two cells harboring the same genotype) and heterotypic (between a control and mutant cell) fusion events were defective, demonstrating the requirement for Srf in both fusion partners. We showed that the lack of Srf perturbed actin cytoskeleton organization in primary cells. We used metal-replica EM on unroofed muscle cells and demonstrated the existence of actin-based finger-like protrusions at the site of fusion, which were absent in fusion-deficient MBs lacking Srf. Strikingly, reestablishment of the actin scaffold in Srf mutant SCs by the overexpression of α-cardiac actin (*Actc1*) restored the heterotypic fusion capacity between control MBs/MTs and mutant MBs, both in vitro and in vivo (upon overload), and overload-induced muscle growth. However, homotypic fusion was not rescued by the maintenance of the actin architecture in cultured mutant cells and in vivo (upon regeneration), suggesting that additional Srf target genes are involved. Altogether, our data provide evidence for the importance of the actin cytoskeleton and actin-based protrusions in MB fusion in vertebrates and for the requirement of SC fusion in growing myofibers to obtain efficient hypertrophic myofiber growth.

Results

Srf in SCs is required for overload-induced hypertrophy

We first examined Srf expression in quiescent and activated adult muscle stem cells. Single fibers and their associated SCs were isolated from extensor digitorum longus (EDL) muscles at steady state and were immediately fixed to evaluate Srf expression in quiescent SCs expressing Pax7 by immunostaining (Fig. 1 A). Srf was poorly expressed in quiescent SCs, as <20% of $Pax7^+$ cells were also Srf^+. In contrast, single fibers maintained for 24 h in culture, to allow the activation of the associated SCs, showed Srf expression in all activated SCs (Fig. 1, A and B).

We investigated the role played by Srf in SCs by inducing CH of the plantaris muscle in control and mutant mice (Fig. 1 C). In our CH procedure, SCs were mobilized without destruction of the myofibers, allowing the study of mutant SC behavior in a wild-type environment. Tamoxifen (TMX) treatment induced efficient loss of Srf transcripts and protein (Fig. S1, C and D) in FACS-sorted SCs from control and mutant muscles (Fig. S1, A and B). At steady state (sham operated [SO]), there was no difference in muscle weight and myofiber cross section area (CSA) between control and mutant muscles (Fig. 1, D–F). After hypertrophy, the plantaris muscle mass and CSA were greater for control overloaded muscles 3 and 5 wk after CH than for unloaded muscles (SO; Fig. 1, D–F). However, the extent of hypertrophic growth was strongly reduced in mutant muscles, displaying only a 10% increase in CSA and 20% in mass versus 50% in controls 3 wk after CH. These changes were not accompanied by modifications of myofiber number (Fig. 1 G), indicating that the increase in muscle mass was mainly caused by myofiber hypertrophy. These data show that Srf expression by SCs is necessary for optimal overload-induced myofiber hypertrophy.

Srf is dispensable for SC proliferation

Srf has been shown to control the proliferation of several cell types including the C2C12 MB cell line (Soulez et al., 1996). We next investigated whether Srf loss altered SC function upon CH by quantifying the number of SCs that express Pax7. Before overload, SC numbers were identical between control and mutant plantaris muscles (Fig. 2 B). 1 wk after CH, there was a significant increase in the number of $Pax7^+$ cells in both control and mutant plantaris muscles, which returned to their original level 5 wk after CH (Fig. 2, A and B). Importantly, no difference in SC number was observed between control and mutant muscles after CH, suggesting that Srf loss did not hamper SC growth response to mechanical cues.

We further assessed the proliferative potential of *Srf*-deleted SCs in vitro by determining S (EdU incorporation), G2, and M phases (phospho-histone-$H3^+$ [$PH3^+$] nuclei) of control and mutant FACS-sorted MBs. In agreement with in vivo observations, the percentages of EdU^+ and $PH3^+$ cells of control and mutant MBs were equivalent, indicating similar proliferation rates (Fig. 2, C and D). We conducted additional experiments in which *Srf* loss was achieved in vitro by transducing primary $Srf^{flox/flox}$ MBs with an adenovirus expressing either the Cre recombinase (Ad-Cre) or GFP (Ad-GFP; Fig. S1 E). Again, there was no difference in the proliferative capacities of Ad-GFP– and Ad-Cre–transduced MBs in BrdU incorporation experiments (Fig. S1 F) and in their distribution in the different cell cycle phases analyzed by FACS quantification of DNA content (Fig.

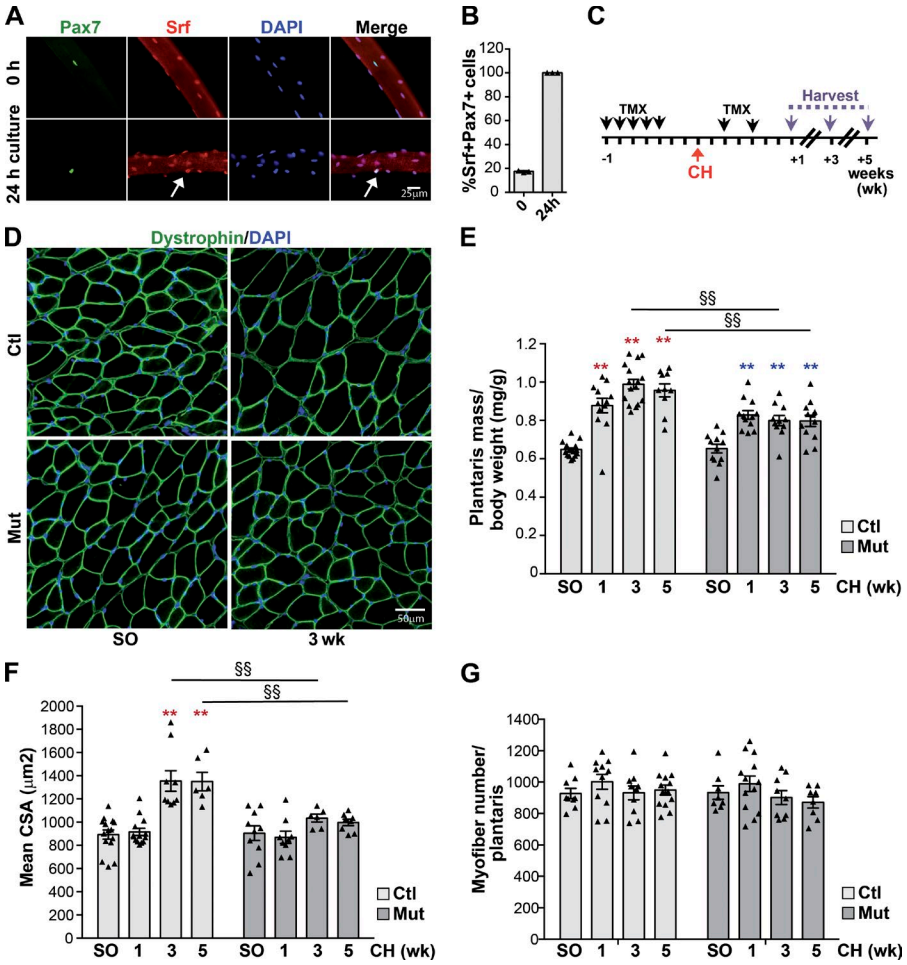

Figure 1. ***Srf* loss in SCs results in CH deficiency in plantaris muscle. (A)** Immunostaining for Pax7 (green) and Srf (red) on single fibers fixed immediately after isolation (0 h) or maintained in culture for 24 h. White arrows indicate SC expressing both Srf and Pax7. **(B)** Proportion of SCs displaying Srf expression ($Pax7^+Srf^+$; $n = 3$). **(C)** Srf mutant mice were injected with TMX 1 wk before CH procedure and after CH. Plantaris muscles were isolated 1, 3, and 5 wk after surgery. **(D)** Plantaris muscle sections immunostained for dystrophin (green) and nuclear staining with DAPI for control and Srf Mutant mice before (SO) and after 3 wk of CH. **(E)** Ratio of plantaris mass (milligrams) to body weight (grams) before (SO) and after 1, 3, and 5 wk of CH in control and Mutant mice (n = 10–16 muscles from n = 6–9 mice). **(F)** Mean CSA (square micrometers) before (SO) and after 1, 3, and 5 wk of CH in control and mutant mice (n = 6–15 muscles from n = 5–9 mice). **(G)** Mean myofiber number before (SO) and after 1, 3, and 5 wk of CH in control and mutant mice (n = 8–14 muscles from n = 6–9 mice). Data are mean ± SEM. **, $P < 0.01$ versus SO; §§, $P < 0.01$.

S1 G). Altogether, these data show that Srf in SCs is dispensable for their proliferation in a cell autonomous manner.

Srf controls SC motility but is not essential for the myogenic differentiation potential of SCs

We reasoned that other SC functions such as motility, differentiation, and fusion could be modified by *Srf* loss and account for the impaired hypertrophic growth of mutant muscle. As Srf is a central regulator of genes involved in cell migration (Esnault et al., 2014), we monitored the motile functions of *Srf*-deleted SCs in vitro using time-lapse videomicroscopy. The motility of mutant and Ad-Cre transduced $Srf^{flox/flox}$ MBs was decreased in comparison to control cells (Figs. 2 E and S1 H), demonstrating that Srf is needed for SC movement.

We next investigated whether *Srf* deletion could affect the myogenic differentiation potential of SCs. Indeed, previous in vitro studies in the C2C12 muscle cell line indicated that Srf activity was required for *MyoD* and *Myogenin* expression and myogenic cell determination and differentiation (Vandromme et al., 1992; Gauthier-Rouviere et al., 1996). We first assessed the number of Myogenin-expressing cells in vivo during overload-induced hypertrophy. After 1 wk of CH, the number of $Myogenin^+$ cells increased similarly in both control and mutant plantaris muscles (Fig. 3 A). In primary cultured muscle cells, MyoD and Myogenin protein and transcript levels did not differ between control and mutant MBs under proliferation conditions or after induction of differentiation (Fig. 3, B and C; and Fig. S1, I and J), in contrast to previous observations in C2C12 cells. We monitored the expression of a late differentiation marker (the sarcomeric myosin heavy chain [MyHC]) in control and mutant cells upon differentiation using the MF20 antibody (Fig. 3 D). The proportion of nuclei in $MyHC^+$ cells was identical between control and mutant cells 3 d postdifferentiation (Fig. 3 E). Collectively, these data show that Srf inactivation in SCs does not impair their engagement in myogenic differentiation.

Srf is crucial for SC fusion capacities

We examined whether the lack of Srf in SCs affects cell fusion by counting the number of myonuclei (DAPI staining) inside the sarcolemma (dystrophin immunostaining) in control and mutant plantaris muscle sections at various times after CH (Fig. 1 D). The number of myonuclei per myofiber was similar before overload between control and mutant muscles and increased significantly in control muscles at 1, 3, and 5 wk after CH. In contrast, myonuclei number did not change in mutant muscles after overload and was significantly reduced compared with controls (Fig. 4 A). To further determine the fusion capacities of SCs in vivo, we assessed fusion through EdU labeling of proliferating cells and by tracking the EdU^+ nuclei incorporated into dystrophin myofibers (Fig. S2, A and B). 3 wk after CH, the percentage of EdU^+ myofibers was blunted in mutant compared with control muscles (Fig. S2 C). Such decreased SC recruitment to the growing myofibers may be attributable to the

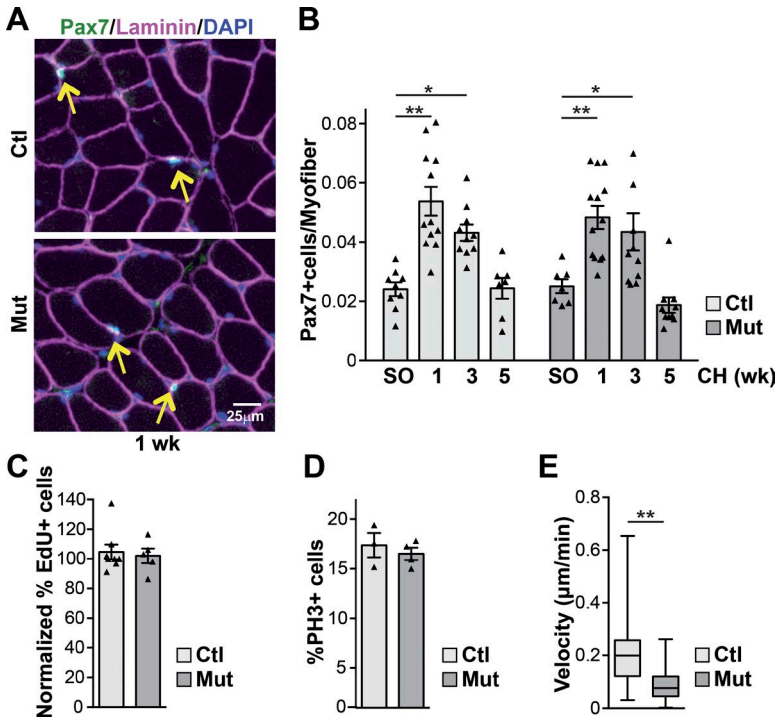

Figure 2. ***Srf* loss within SCs does not affect their proliferation but impairs their motility. (A)** control and Srf mutant plantaris muscle section immunostained for Pax7 (green), laminin (magenta), and nuclear staining with DAPI 1 wk after CH. Yellow arrows indicate Pax7-expressing SCs. **(B)** Number of Pax7+ cells per myofiber in control and mutant plantaris muscle sections before (SO) and after 1, 3, and 5 wk of CH (n = 7–12 muscles from n = 4–7 mice). **(C)** Normalized percentage of EdU+ cells in control and mutant FACS-sorted SCs cultured in rich medium for 5 d (n = 8–5 mice). **(D)** Percentage of PH3+ cells in control and mutant FACS-sorted SCs cultured in rich medium for 5 d (n = 3–4 mice). **(E)** Mean velocity (micrometers per minute) of control and mutant MBs determined by time-lapse videomicroscopy (one representative experiment). Data are means ± SEM. *, P < 0.05; **, P < 0.01.

dampened fusion capacity of SCs lacking Srf, as both number and proliferative capacity of SCs were unaffected by *Srf* loss.

Srf mutant cells showed an altered capacity to form multinucleated MTs 3 d after induction of differentiation (Figs. 3 D and 4 B). Their fusion index, which represents the proportion of the total cell population that fused, was lower than that of control cells (Fig. 4 C). Accordingly, the mean number of nuclei in differentiated MyHC+ cells was much lower in mutant than

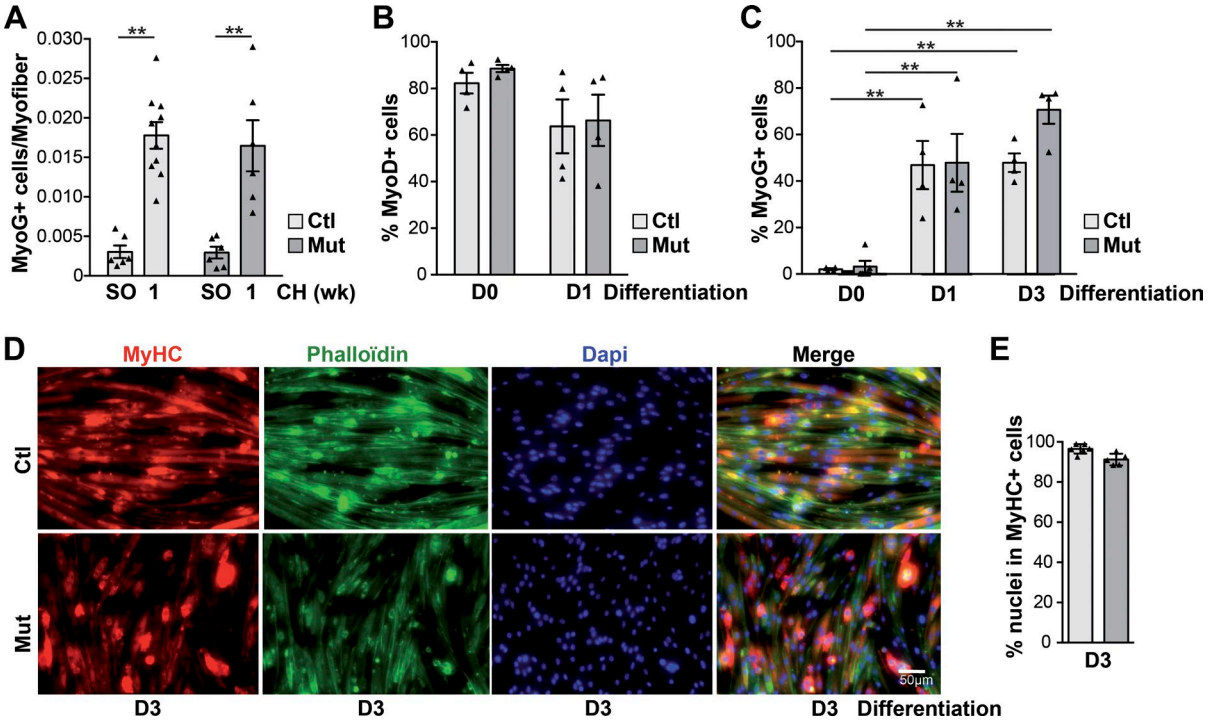

Figure 3. ***Srf* loss does not affect myogenic differentiation of SCs. (A)** Number of MyoG+ cells per myofiber in control and Srf mutant plantaris muscle sections before (SO) and after 1 wk of CH (n = 6–10 muscles from n = 4–6 mice). **(B)** Percentage of MyoD+ cells in control and mutant FACS-sorted SCs cultured in rich medium (D0, MBs) or 1 d after differentiation induction (D1; n = 4). **(C)** Percentage of MyoG+ in control and mutant FACS-sorted SCs cultured in rich medium (D0) or 1 (D1) and 3 (D3) days after differentiation induction (n = 4–5). **(D)** Immunostaining for MyHC, nuclear staining with DAPI, and F-actin staining with phalloidin on control and mutant cells 3 d after differentiation induction. **(E)** Percentage of nuclei in MyHC+ cells in control and mutant cells 3 d after differentiation induction (n = 5–6). Data are mean ± SEM. **, P < 0.01.

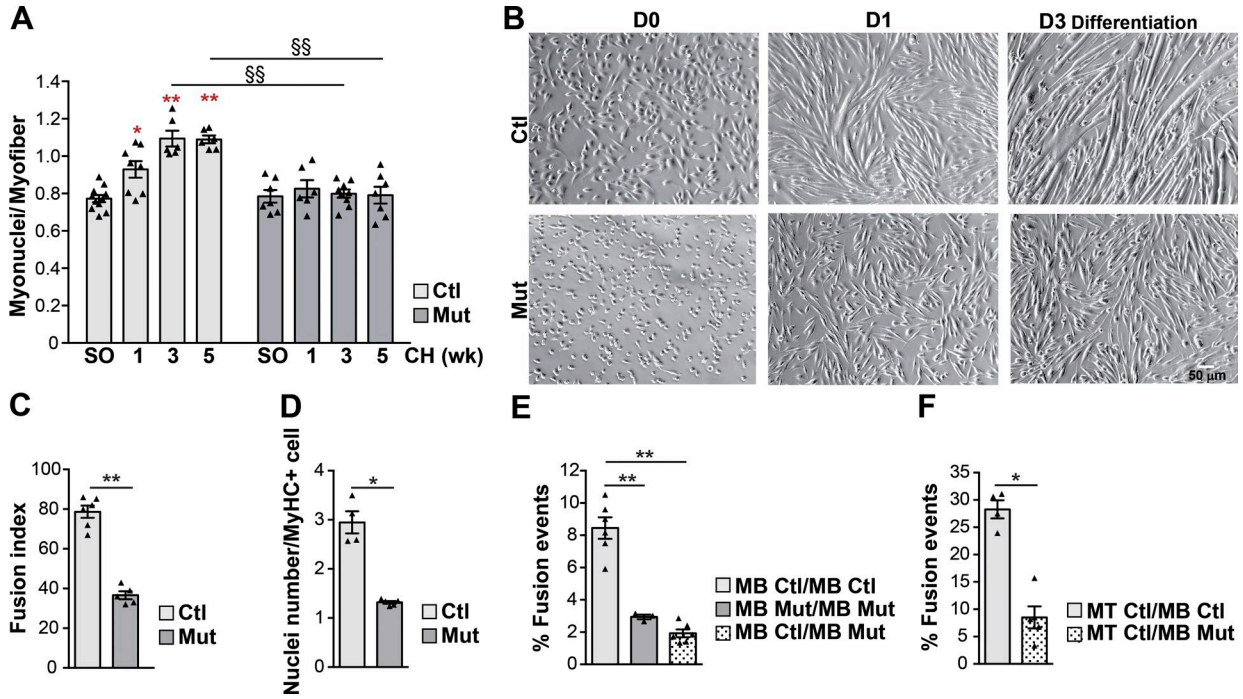

Figure 4. **Srf controls SC fusion. (A)** Number of nuclei (DAPI) within the dystrophin+ sarcolemma per myofiber before (SO) and after 1, 3, and 5 wk of CH in control and Srf mutant plantaris muscles (n = 6–11 muscles from n = 4–6 mice). Data are mean ± SEM. *, P < 0.05 versus SO; **, P < 0.01 versus SO; §§, P < 0.01. **(B)** Phase-contrast representative pictures of FACS-sorted control and mutant SCs cultured in rich medium (D0) or 1 (D1) and 3 (D3) days after differentiation induction. **(C)** Proportion of nuclei within multinucleated cells (fusion index) in control and mutant cells 3 d after differentiation (n = 5–6). **(D)** Mean number of nuclei per MyHC+ cell in control and mutant cells induced to differentiate for 3 d (n = 4–5). **(E)** Control and mutant MB were labeled with Orange Cell Tracker and mixed with control or mutant MBs labeled with Deep Red Cell Tracker. After 48 h of co-culture in differentiation medium, the percentage of dual-labeled MTs per total number of nuclei was scored (n = 3–6). **(F)** MT control were labeled with Orange Cell Tracker and mixed with MB control or MB mutant labeled with Deep Red Cell Tracker. After 48 h of co-culture, the percentage of dual-labeled MTs per total number of cells was scored (n = 4–5). For C–F, data are mean ± SEM. *, P < 0.05; **, P < 0.01.

control cells (Fig. 4 D). We then evaluated whether heterotypic MB fusion, between a control and a mutant MB, was also affected by performing cell mixing experiments of cells labeled with two different fluorescent dyes. We confirmed that mutant MBs were unable to fuse in a homotypic manner (between two mutant cells), as there were fewer fusion events (dual labeling) between mutant MBs than between control MBs (Fig. 4 E, lane MB Mut/MB Mut). Mutant MBs also exhibited highly diminished heterotypic fusion with control cells (Fig. 4 E, lane MB control/MB Mut). We then studied the fusion between MBs and MTs (MT/MB) by cell mixing of differently labeled cells. The lack of Srf in MBs was accompanied by a large decrease in fusion events (Fig. 4 F, lane MT control/MB mutant), showing that MBs require Srf for fusion to control MTs, a process that may lead to the accretion of new nuclei into myofibers upon overload-induced hypertrophy in vivo.

Altogether, these results show that Srf within MBs is indispensable for homotypic and heterotypic fusion events, indicating that Srf expression is required in both fusing cells. In addition, our results suggest that the decreased ability of SCs lacking Srf to fuse with the growing fibers could account for the defective hypertrophic growth of mutant muscles.

Srf-deleted MBs display impaired actin cytoskeleton organization and an absence of actin based finger-like protrusions at the site of fusion

We next sought to identify Srf target genes that could participate in the control of SC motility and fusion by performing a microarray analysis of gene expression in muscle cells expressing Srf (Ad-GFP) or not (Ad-Cre). We identified a set of 144 genes whose expression was altered by Srf loss in both proliferating MBs (D0) and differentiating cells (D1 and D3; Fig. 5 A and Table S1). Analysis of the potential biological functions of these genes by a gene ontology program (Ingenuity) pointed out an overrepresentation of genes involved in the regulation of actin cytoskeleton signaling (Fig. 5 B). We further focused our attention on several validated Srf direct genes including actin genes and genes implicated directly or indirectly in actin cytoskeleton regulation such as *Abra*, *Cnn2*, *Fermt2*, *FlnA*, *Tgfb1i1*, and *Wdr1* (Wang et al., 2011; Chong et al., 2012; Esnault et al., 2014). In line with the transcriptomic data, we confirmed by qRT-PCR that the expression of actin isoforms (including α-skeletal actin [*Acta1*], α-cardiac actin [*Actc1*], β-actin [*Actb*], γ-actin [*Actg*], and smooth muscle actin [*Acta2*]) and of *Abra*, *Cnn2*, *Fermt2*, *FlnA*, *Tgfb1i1*, and *Wdr1* genes was strongly diminished in cells lacking Srf (Fig. 5, C and D; and Fig. S2, D and E). Altogether, these expression studies show that, in muscle cells, expression of both structural components and regulators of actin network are affected by Srf deletion, suggesting that actin scaffold structures may be altered in Srf mutant cells, which may account for their perturbed functions.

We then quantified the total amount of F-actin per cell in control and mutant MBs by phalloidin staining (Fig. 6 A) and showed a significant reduction of total F-actin in mutant cells (Fig. 6 B). As the decrease of total F-actin per cell could be caused by the decrease of the total amount of actin in the cell or the

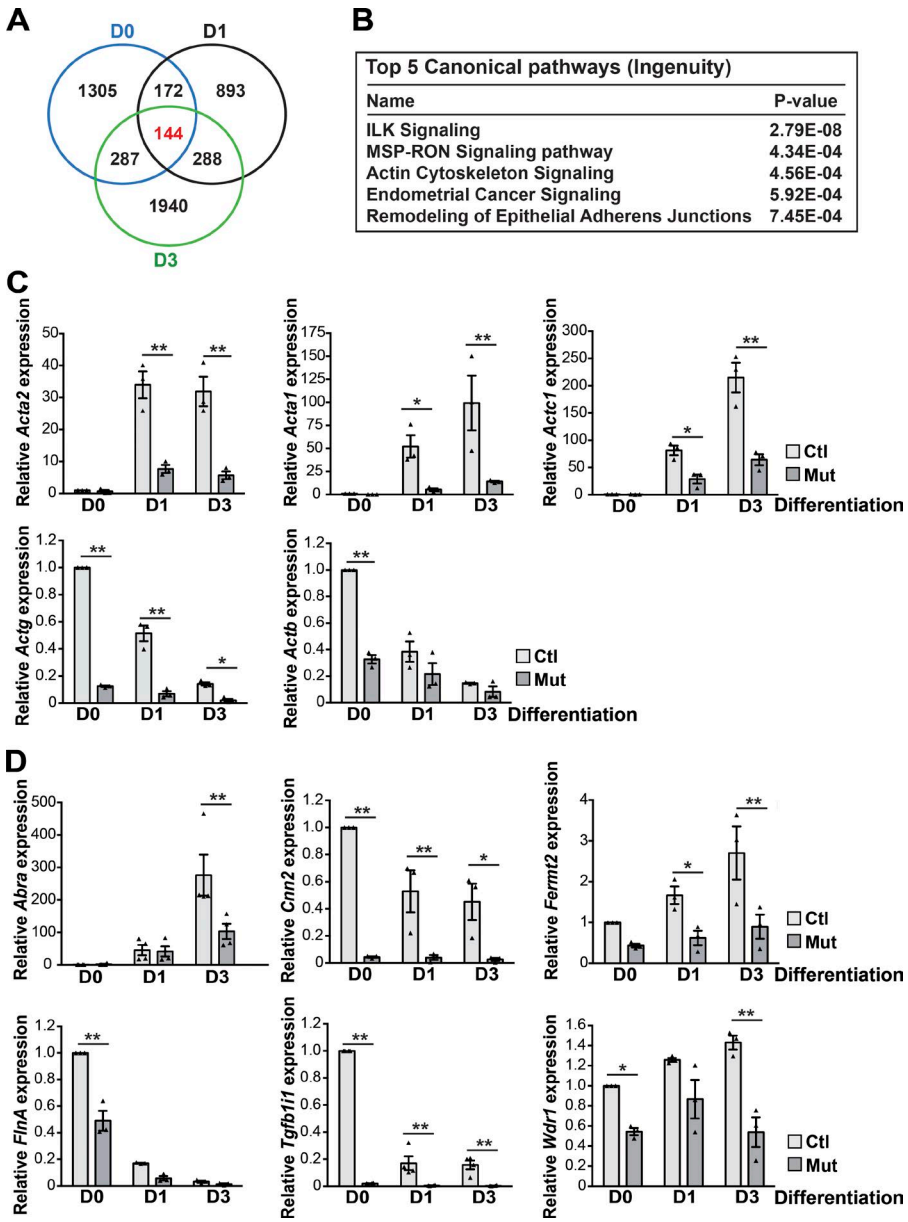

Figure 5. **Srf controls the expression of actin genes and genes implicated in actin cytoskeleton regulation. (A)** Venn diagram showing the intersections between genes differentially regulated by Srf ($P < 0.05$) in MBs (D0), myocytes at onset of differentiation (D1), and differentiated cells (D3). In red is indicated the number of genes (144) that are modulated by Srf independently of the differentiation state. **(B)** Top five canonical pathways identified by gene ontology analysis using Ingenuity of the 144 common genes whose expression is Srf dependent. **(C)** Analysis of *α-skeletal actin* (*Acta1*), *α-cardiac actin* (*Actc1*), *smooth muscle actin* (*Acta2*), *γ-actin* (*Actg*), and *β-actin* (*Actb*) mRNA expression by qRT-PCR in FACS-sorted control and Srf mutant SCs cultured in rich medium (D0) or 1 (D1) and 3 (D3) days after differentiation. Data were normalized by *Hmbs* expression and relative to D0 ($n = 3$). **(D)** Analysis of *Abra*, *Cnn2*, *Fermt2*, *FlnA*, *Tgfb1i1*, and *Wdr1* mRNA expression by qRT-PCR in FACS-sorted control and mutant SCs cultured in rich medium (D0) or 1 (D1) and 3 (D3) days after differentiation. Data were normalized by *Hmbs* expression and relative to D0 ($n = 3$). Data are mean ± SEM. *, $P < 0.05$; **, $P < 0.01$.

diminished proportion of the total pool of actin that is polymerized (F-actin), we first quantified total actin by Western blot using an antibody recognizing all actin isoforms and showed a sharp reduction of total actin quantity in mutant primary MBs compared with controls (Fig. 6, C and D). Furthermore, we quantified soluble G-actin and insoluble F-actin fractions in muscle cells; the F/G-actin ratio in MBs lacking Srf was reduced to 40% of control cell levels (Fig. 6, E and F). Thus, the decreased F-actin amount in mutant primary MBs could be attributed to both diminished total actin and altered regulation of actin polymerization.

We sought to obtain additional insights into the precise organization of the actin cytoskeleton in control and mutant primary MBs by confocal microscopy (Fig. 6 G) and metal-replica EM on unroofed muscle MBs (Fig. 6, H and I). The latter technique enabled us to visualize the ultrastructure of the actin cytoskeleton at the ventral membrane of the cell at high resolution. The actin cytoskeleton associated with the ventral membrane in control cells presented an organization that included both stress fibers formed from actin cables/bundles and branched actin (Fig. 6, G [bottom], H, H′, and H″; and Fig. S3, B, C, and C′). Srf mutant cells contained fewer and abnormally oriented actin cables (Fig. 6, G [bottom], I, I′, and I″; and Fig. S3, D, E, and E′). Accordingly, there was less intense cortical F-actin staining in mutant MBs than controls progressing toward the top of the cell on confocal *z*-sections (Fig. 6 G, middle and top). These results collectively show that Srf controls actin cytoskeleton organization (in actin cables) in cultured muscle cells.

It is possible that the altered actin organization of mutant MBs is responsible for their compromised fusion capacity. In *Drosophila*, podosome-like structures were shown to form at the "fusing" synapse (Martin, 2016). To visualize putative F-actin remodeling at the site of cell–cell fusion, we labeled primary myocytes with SiR-actin, a live fluorogenic cell F-actin probe, and performed time-lapse videomicroscopy upon differentiation. After tracking the fusion events using bright field (Fig. S3 A′ and Video 1), F-actin rearrangements were observed at the cell–cell contact at the fusion site (Fig. S3 A and Video 2). To visualize cellular and actin-based structures at the

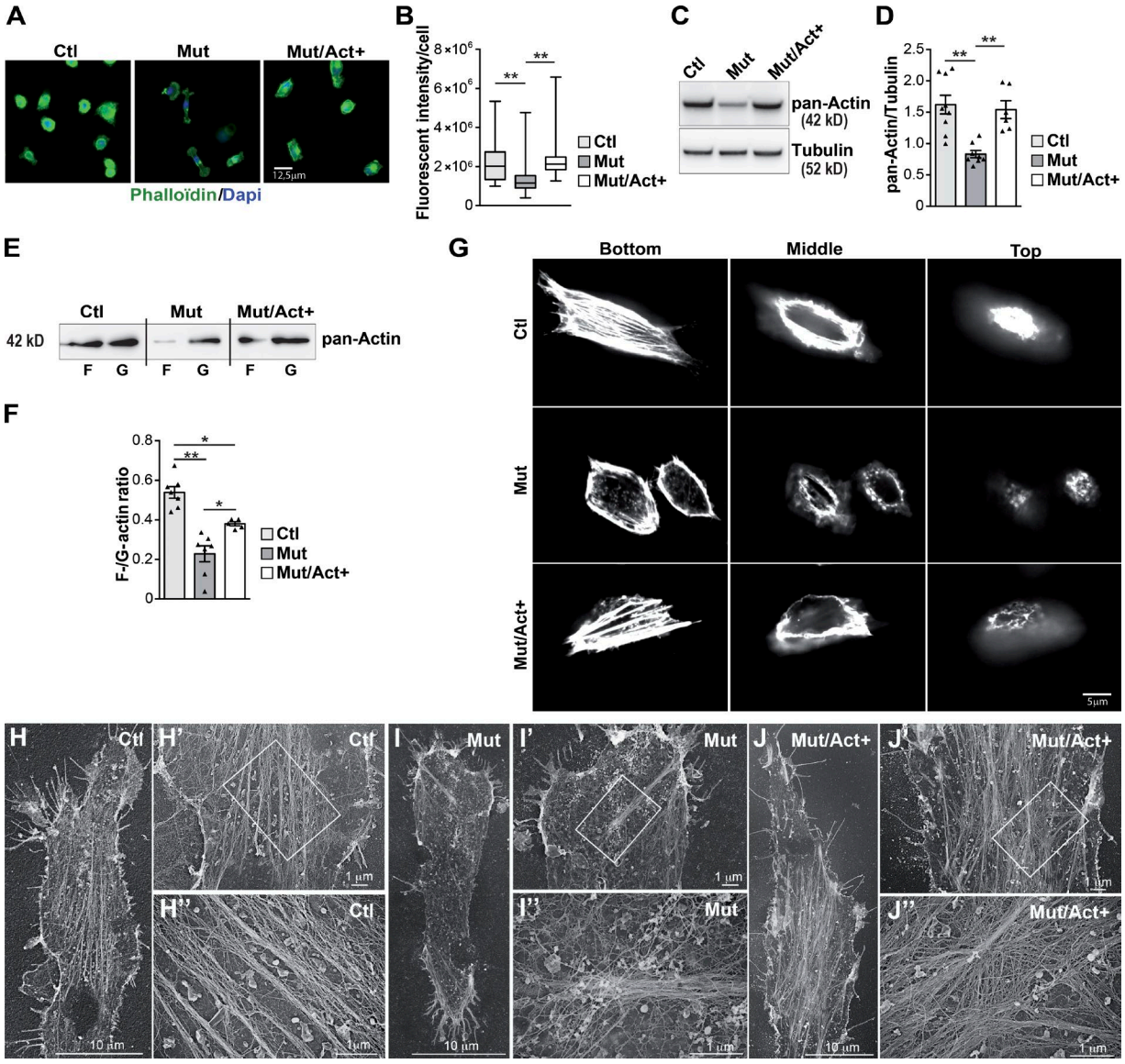

Figure 6. **α-Actin overexpression restores the impaired F-actin content of *Srf*-deleted MBs. (A)** Staining for F-actin (phalloidin) and nuclei (DAPI) on control, *Srf*-deleted (Mut), and *Srf*-deleted MBs overexpressing α-actin (Mut/Act+). **(B)** Quantification of F-actin by measuring the total phalloidin fluorescence intensity per cell (ImageJ) in control, mutant, and Mut/Act+ MBs (one representative experiment). **(C)** Representative immunoblot showing total actin (pan-Actin) in control, mutant, and Mut/Act+ MBs. Tubulin was used as a loading control. **(D)** Quantification of the pan-actin/tubulin ratio from immunoblots (n = 5–9). **(E)** Representative immunoblot showing actin in the insoluble (F) versus soluble (G) fractions in control, mutant, and Mut/Act+ MBs. **(F)** Quantification of the F-/G-actin ratio from immunoblots (n = 6–8). **(G)** Representative confocal projections of z-sections of F-actin staining (phalloidin) taken from the adherent (ventral) cell bottom and middle and proceeding up to the media-facing top of control, mutant, and Mut/Act+ MBs. **(H)** Survey view of the cytoplasmic surface of the plasma membrane from unroofed control MBs. **(H′)** Higher-magnification view from H. **(H″)** Higher-magnification view corresponding to the boxed regions in H′. **(I)** Survey view of the cytoplasmic surface of the plasma membrane from unroofed mutant MBs. **(I′)** Higher-magnification view from I. **(I″)** Higher-magnification view corresponding to the boxed regions in I′. **(J)** Survey view of the cytoplasmic surface of the plasma membrane from unroofed Mut/Act+ MBs. **(J′)** Higher-magnification view from J. **(J″)** Higher-magnification view corresponding to the boxed region in J′. Data are mean ± SEM. *, P < 0.05; **, P < 0.01.

basal membrane of fusing SCs at higher resolution, we used metal-replica EM in primary myocytes cultured for 24 h in differentiation medium. In control cells, we consistently observed the formation of finger-like actin-based protrusions at the site of prefusion. The electron density of these structures made them easily traceable even when located below the plasma membrane of the acceptor cell (Fig. 7, A, A′, and B). This feature allowed us to analyze "en face" the fusion process, which appears to be directional, as these protrusions occurred only in one cell (cell 1 in Fig. 7 A). The protrusions emanating from a first cell and which were composed of actin cables (white arrow) extended underneath the plasma membrane of the second cell (Fig. 7 B). Of note, we often observed branched actin filaments (indicated by an asterisk in Fig. 7 B) at the base of the actin cable forming the protrusion. In some instances, we observed complete fusion of the plasma membranes (Fig. 7, C and C′) and could visualize the protrusion below the fused membrane (Fig. 7 C′, yellow arrows). Strikingly, these finger-like structures were absent in fusion-deficient MBs lacking Srf and no fusion event was observed out of hundreds of contacting MBs

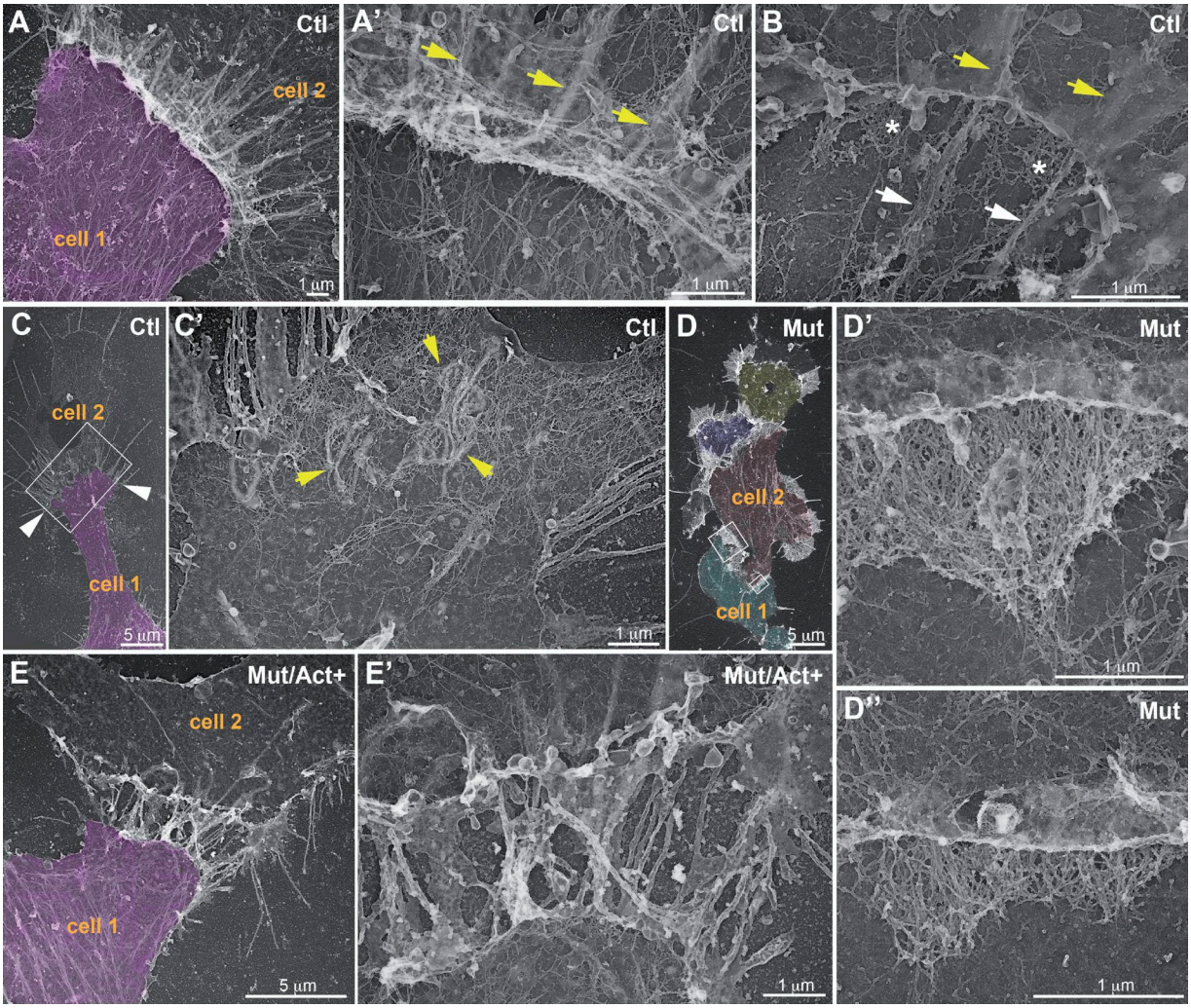

Figure 7. **Formation of finger-like actin-based protrusions at the site of fusion. (A)** Survey view of the cytoplasmic surface of the plasma membrane from control muscle cells differentiated for 24 h. Cell 1: Pseudocolored in purple forms finger-like protrusions that are traceable below the acceptor cell 2. **(A′)** Higher-magnification view from A of the finger-like protrusions denoted with yellow arrows. **(B)** Higher-magnification view of the finger-like protrusions from a double unroofed cell–cell contact. White arrows, actin cables from attacking cell 1; yellow arrows, finger-like protrusions traceable below cell 2; *, branched actin filaments. **(C)** Survey view of the cytoplasmic surface of the plasma membrane from two unroofed control muscle cells differentiated for 24 h that have successfully fused. Cell 1 presenting the protrusions is pseudocolored in purple. White arrowheads denote the fusion site. **(C′)** Higher-magnification view of the fusion site from boxed region in C. Yellow arrows denote finger-like protrusions below the fusion site. **(D)** Survey view of the cytoplasmic surface from mutant muscle cells differentiated for 24 h. Note clusters of MBs (each MB is a different pseudocolor) unable to fuse. **(D′ and D″)** Higher-magnification views of cell contact sites from the boxed regions in C. **(E)** Survey view of the cytoplasmic surface from Mut/Act$^+$ cells differentiated for 24 h. **(E′)** Higher-magnification view from E.

(Fig. 7, D, D′, and D″). Instead of actin cables, there was an accumulation of branched actin at the site of contact between mutant cells suggesting that the inability to form protrusions may be inefficiently compensated by branched actin accumulation (Fig. 7, D′ and D″).

Altogether, these observations show the presence of actin-based protrusions at the cell–cell contact between fusing cells that correlates with the fusogenic capacity of differentiating MBs and suggest that such structures may be required to drive fusion.

Impaired actin cytoskeleton organization in *Srf*-deleted MBs is rescued by the compensatory expression of an α-actin isoform

α-Cardiac (Actc1) and α-skeletal (Acta1) actins have redundant roles in skeletal muscle, as Actc1 overexpression can functionally replace Acta1 in *Acta1* knockout mice (Nowak et al., 2009). Thus, we hypothesized that the perturbed organization of the actin cytoskeleton in Srf-deleted muscle cells could be counteracted by Actc1 overexpression. We generated a mouse model in which *Srf* deletion and *Actc1* expression can be achieved specifically in SCs upon TMX treatment (Mut/Act$^+$ mice; Fig. S4, A and B). The overexpression of *Actc1* in *Srf*-deleted MBs was sufficient to restore the total amount of F-actin per cell (Fig. 6, A and B), the total amount of actin (Fig. 6, C and D), and the F/G-actin ratio (Fig. 6, E and F) to control levels. Confocal microscopy (Fig. 6 G, bottom) and metal-replica EM (Fig. 6, J, J′, and J″) revealed that Mut/Act$^+$ MBs contained more abundant F-actin structures at the ventral membrane, mainly organized in actin cables, than mutant cells, comparable to those in control MBs. Nevertheless, the amount of cortical actin, progressing toward the top of the cell, was similar in Mut/

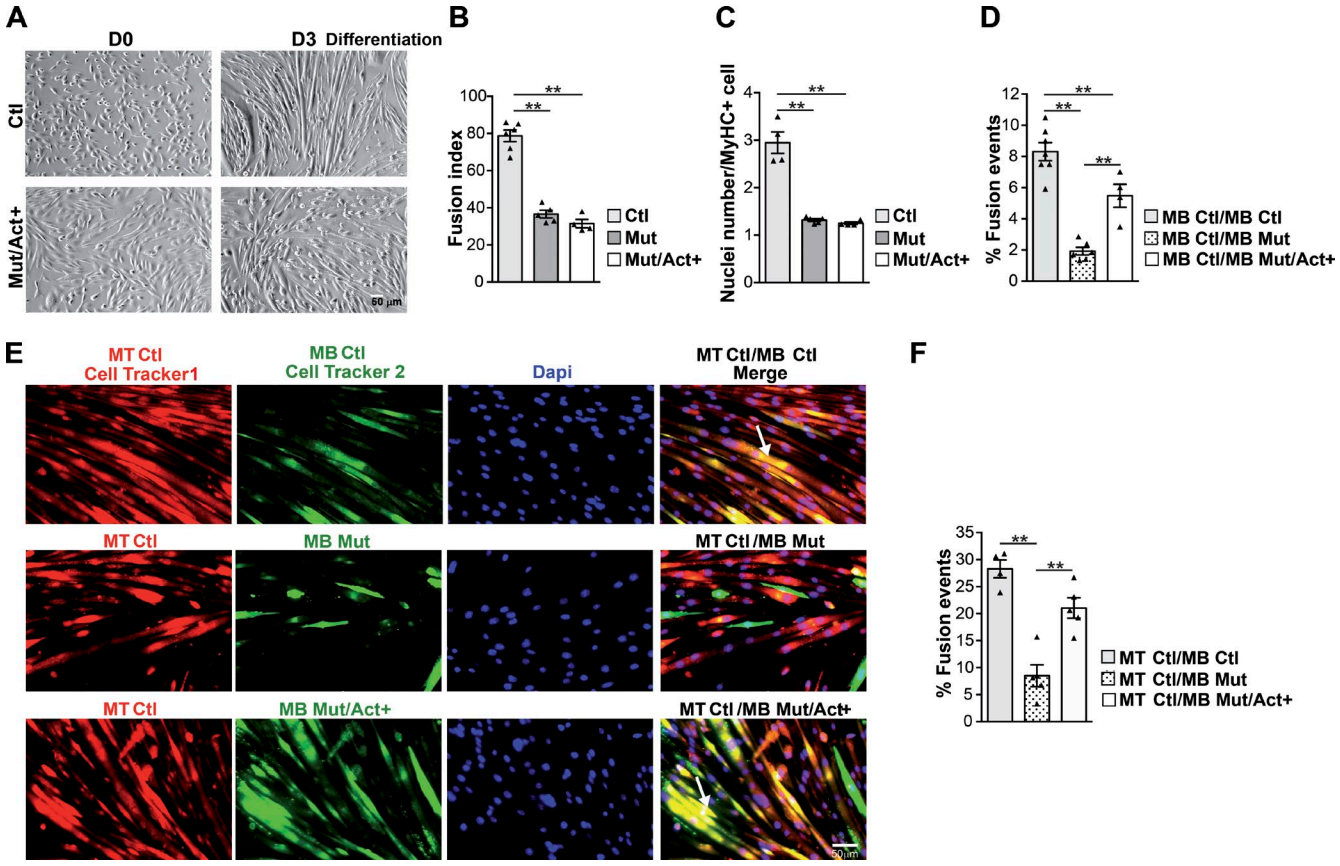

Figure 8. **α-Actin overexpression in MBs lacking Srf restores heterotypic fusion. (A)** Phase-contrast representative pictures of FACS-sorted control and Mut/Act+ SCs cultured in rich medium (D0) or 3 d after differentiation induction (D3). **(B)** Proportion of nuclei within multinucleated cells (fusion index) in control, mutant, and Mut/Act+ cells 3 d after differentiation (n = 4–7). **(C)** Mean number of nuclei per MyHC+ cell in control, mutant, and Mut/Act+ cells induced to differentiate for 3 d (n = 4–5). **(D)** MB control, MB mutant, or MB Mut/Act+ were labeled with Green Cell Tracker and mixed with control MBs labeled with Orange Cell Tracker. After 48 h of co-culture in differentiation medium, the percentage of dual-labeled MTs per total number of nuclei was scored (n = 4–7). **(E)** MT control were labeled with Cell Tracker 1 (Orange; visualized in red) and mixed with MB control, MB mutant, or MB Mut/Act+ labeled with CellTracker 2 (Deep Red; visualized in green). After 48 h of co-culture, MTs were analyzed for dual labeling (indicated by arrow). **(F)** MT control were labeled with Orange Cell Tracker and mixed with MB control, MB mutant, or MB Mut/Act+ labeled with Deep Red Cell Tracker. The percentage of dual-labeled cells per total number of cells was scored (n = 4–5). Data are mean ± SEM. **, P < 0.01.

Act+ and mutant MBs and less abundant than in control cells, suggesting that *Actc1* overexpression did not reestablish all actin structures (Fig. 6 G, middle and top). Collectively, these data demonstrate that α-actin isoform overexpression in SCs lacking Srf is sufficient to partially rescue the altered actin cytoskeleton organization observed in the mutant cells.

α-Cardiac actin overexpression rescues the heterotypic fusion defect caused by Srf loss in MBs

We next investigated whether the reestablishment of actin cytoskeleton in Srf mutant SCs by Actc1 overexpression could rescue defective SC functions, such as motility and fusion. Cell tracking experiments showed a similar decrease of motility in Mut/Act+ and mutant MBs relative to control cells (Fig. S4 C), precluding the involvement of α-actin–mediated F-actin stabilization in the impaired motile functions of SCs lacking Srf.

We then assessed the fusion capacity of Mut/Act+ cells during differentiation. As observed for Srf mutant cells, Mut/Act+ cells displayed an unaltered engagement in differentiation compared with control cells (Fig. S4, D, E, and F). However, upon differentiation, the fusion index and the mean number of nuclei per MyHC-expressing cell were reduced to a similar extent in Mut/Act+ and in Srf mutant cells, suggesting that actin overexpression did not alleviate the homotypic fusion defect of cells lacking Srf (Fig. 8, A–C). Although Mut/Act+ MBs could form numerous filopodia-like structures at the site of cell contact, these protrusions did not successfully extend below the ventral membrane of the contacting cell (Fig. 7, E and E′; and Fig. S3, F, G, and G′).

In contrast, impaired heterotypic fusion between control and Srf mutant MBs and between control MTs and mutant MBs was partially rescued in vitro by *Actc1* overexpression, as assessed by counting the fusion event in cell mixing experiments (Fig. 8, D [lane MB control/MB Mut/Act+], E, and F [lane MT control/MB Mut/Act+]). Importantly, the rescue of fusion in these cells is not accompanied by the restoration of their migratory capacities, highlighting the potential separation of the motility and fusion mechanisms. Overall, these data suggest that the maintenance of the F-actin network in Srf mutant MBs by α-actin overexpression is sufficient to rescue their heterotypic fusion with control MBs/MTs, providing genetic evidence for the requirement of actin-based protrusion in the control of SC fusion. However, actin overexpression was insufficient for homotypic fusion between Srf mutant SCs, indicating that additional Srf target genes must be expressed in at least one of the fusing cells to allow fusion to occur.

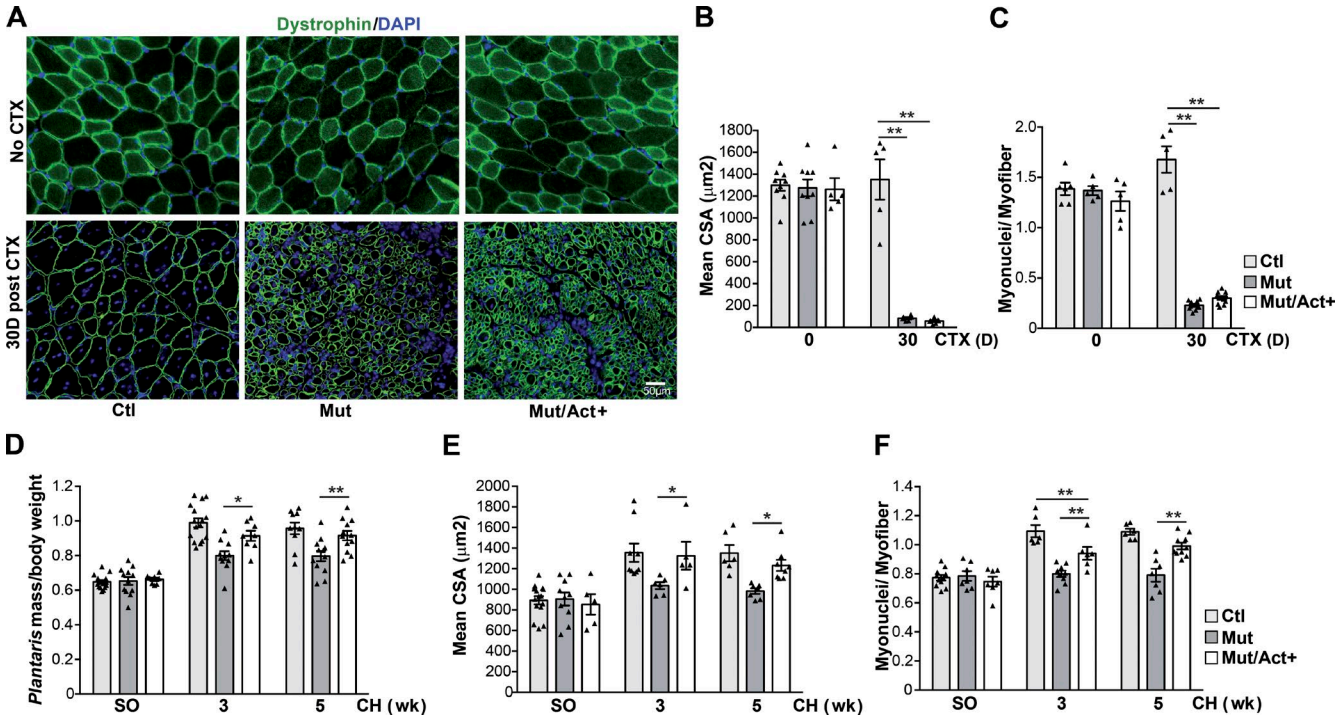

Figure 9. **α-Actin overexpression in Srf-deleted SCs rescues fusion and hypertrophic growth upon overload. (A)** TA muscle sections immunostained for dystrophin (green) and nuclear staining with DAPI for control, mutant, and Mut/Act+ mice untreated (No CTX) and 30 d after CTX-induced muscle injury (30D after CTX). **(B)** Mean CSA (square micrometers) of TA muscles untreated (0) and 30 d after CTX-induced injury in control, mutant, and Mut/Act+ mice (n = 5–9 muscles from n = 4–7 mice). **(C)** Number of nuclei (DAPI) within the dystrophin+ sarcolemma per myofiber in untreated (0) and 30 d after CTX-induced injury of control, mutant, and Mut/Act+ TA muscles (n = 5–11 muscles from n = 4–7 mice). **(D)** Ratio of plantaris mass (milligrams) to body weight (grams) before (SO) and after 3 and 5 wk of CH in control, mutant, and Mut/Act+ mice (n = 5–16 muscles from n = 4–9 mice). **(E)** Mean CSA (square micrometers) of plantaris before (SO) and after 3 and 5 wk of CH in control, mutant, and Mut/Act+ mice (n = 5–15 muscles from n = 4–9 mice). **(F)** Number of nuclei (DAPI) within the dystrophin+ sarcolemma per myofiber before (SO) and after 3 and 5 wk of CH in control, mutant, and Mut/Act+ plantaris muscles (n = 6–11 muscles from n = 4–6 mice). Data are mean ± SEM. *, P < 0.05; **, P < 0.01.

α-Cardiac actin overexpression in Srf mutant muscles does not rescue homotypic fusion in vivo upon regeneration

We conducted muscle regeneration experiments, recapitulating homotypic fusion events on control, mutant, and Mut/Act+ mice. Upon cardiotoxin (CTX)-induced injury, SC fusion occurs exclusively between cells of the same genotype. Dystrophin/DAPI staining of regenerated tibialis anterior (TA) muscle sections showed the overall structure of Srf mutant muscles to be severely affected relative to control muscles 30 d after CTX injection (Fig. 9 A). Indeed, the newly formed fibers in mutant muscles were 10 times smaller (Fig. 9 B) and three times more numerous than those in control muscles (Fig. S5 A). Moreover, there were far fewer myonuclei in mutant regenerated muscles than in control muscles (Fig. 9 C). Of note, the number of SCs was not affected by *Srf* loss 30 d postinjury (Fig. S5 B). Overall, these data suggest a strong deficiency of *Srf*-deleted SCs fusion that could account for the small size and the increased number of regenerated fibers present in mutant muscles.

We next assessed whether α-actin overexpression could counteract the altered regeneration and defective homotypic fusion of regenerated Srf mutant muscles. There was no improvement of fusion and mean CSA in Mut/Act+ relative to Srf mutant muscles 30 d postinjury (Fig. 9, B and C). These data are in accordance with the absence of an improvement of the homotypic fusion defect observed in vitro in Mut/Act+ MBs relative to Srf mutant cells (Fig. 8, B and C).

α-Cardiac actin overexpression restores overload-induced hypertrophic muscle growth of Srf mutant muscles

Heterotypic fusion between mutant or Mut/Act+ MBs and control MTs models the nuclear accretion that occurs in vivo during overload-induced hypertrophy. We thus determined the impact of α-actin overexpression on the defective hypertrophy of Srf mutant muscles. Actin overexpression rescued the overall growth of Srf mutant muscles to control levels 3 and 5 wk after CH. Indeed, Mut/Act+ plantaris muscle mass and mean CSA were significantly higher than those of Srf mutant muscles and were comparable to those of control muscles (Fig. 9, D and E). Furthermore, there were significantly more myonuclei in Mut/Act+ than in Srf mutant muscles, reaching 60% of control levels 5 wk after CH (Fig. 9 F). Accordingly, 3 wk after CH and after in vivo EdU labeling, the percentage of myofibers that incorporated EdU+ nuclei was significantly increased in Mut/Act+ muscles compared with Srf mutant muscles (Fig. S2 C). These data demonstrate that the maintenance of a filamentous actin scaffold within SCs lacking Srf was sufficient to efficiently drive heterotypic fusion in vitro and restore the impaired hypertrophic growth of Srf mutant muscles in vivo.

Discussion

Taking advantage of a genetic model that allows the specific deletion of Srf in adult muscle stem cells, we show in vivo and

in vitro that Srf is a master regulator of SC fusion, whereas it is dispensable for their proliferation and differentiation. Furthermore, we used both metal-replica EM on unroofed muscle cells and a genetic model of α-actin overexpression to provide evidence on how actin cytoskeleton architecture affects SC fusion in mammals.

Srf activates *MyoD* expression, MB proliferation, and differentiation in the C2C12 muscle cell line (Gauthier-Rouviere et al., 1996; Soulez et al., 1996; Carnac et al., 1998), and the distal regulatory region of the *MyoD* gene contains a shared MEF2/Srf binding element (L'honore et al., 2003). In addition, skeletal muscle–specific deletion of Srf coactivators Mrtf-A and Mrtf-B during embryonic development impaired MB proliferation and increased apoptosis (Cenik et al., 2016). In contrast to these previous studies, our results show that SCs lacking Srf respond to mechanical cues by expanding their number similarly to control SCs and that their cell cycle progression is unaffected ex vivo. Moreover, *Srf* loss in primary cell culture did not perturb MyoD expression. The discrepancy between our results and those obtained with the C2C12 cell line and embryonic progenitors may be attributable to differences between cell lines and primary cells and muscle progenitors isolated from either adult muscles (our study) or embryonic muscles (study on Mrtfs deletion; Cenik et al., 2016). SC-specific deletion of both *MASTR* and *Mrtf-A* leads to excessive proliferation of SCs because of the down-regulation of *MyoD* expression (Mokalled et al., 2012). The authors of the study proposed that MEF2 transcription factor, and its associated MASTR cofactor, cooperate with Mrtf-A to regulate the transcriptional regulation of *MyoD* expression (Mokalled et al., 2012). Thus, it is possible that *MyoD* expression is mainly controlled by the MASTR/MEF2 pathway in *Srf*-deleted SCs.

Previous in vitro studies using the C2C12 cell line showed that the myogenic differentiation was impaired by inhibition of Srf (Gauthier-Rouviere et al., 1996; Soulez et al., 1996). However, in the present study, the number of Myogenin-/MyHC-expressing cells was not affected by *Srf* loss in cultured primary MBs under differentiation conditions or during overload-induced hypertrophy in vivo, indicating that Srf activity is not required for MB engagement into the differentiation program. In contrast, we identified Srf to be a major regulator of the fusion process. Indeed, the absence of Srf in SCs led to the formation of small MTs containing very few nuclei during differentiation in culture, small and numerous myofibers during in vivo regeneration, and the absence of nucleus accretion during myofiber hypertrophic growth. Our results are in accordance with the altered fusion observed in muscles lacking Srf cofactors Mrtf-A and Mrtf-B (Cenik et al., 2016).

Studies conducted in *Drosophila* and vertebrate systems led to a model for MB fusion. Three major phases accompany the MB fusion process: (a) the initial event of adhesive interactions between cells, (b) the recruitment of the actin-polymerization machinery to the membrane and the formation of transient actin-based structures, and (c) the formation of discontinuities and the merging of the apposed membranes (Kim et al., 2015a; Schejter, 2016). The contribution of the actin-polymerization machinery in mammalian MB fusion has been described using knockout models (Cdc42, Rac1, and N-WASp; Vasyutina et al., 2009; Gruenbaum-Cohen et al., 2012), but specific actin structures at the site of fusion, including cortical branched-actin and invasive extensions, have been described mainly in *Drosophila* (Sens et al., 2010; Dhanyasi et al., 2015; Segal et al., 2016). Our data provide the first description of discrete actin-based structures whose presence correlates with the fusion capacities of primary vertebrate MBs. Actin-rich protrusions have been previously described in differentiating C2C12 MBs, but there was no evidence of the presence or absence of such structures in fusion-incompetent cells (Shin et al., 2014). Using live imaging, we show the F-actin remodeling at the cell–cell contact of primary myocytes before fusion. EM analysis allowed us to directly visualize these structures and show that they form finger-like actin-based protrusions that are asymmetrically distributed and are composed of actin filament cables with branched actin networks at their base. These protrusions have the unique feature of crawling underneath the "receiving" cell, making them difficult to visualize by EM techniques that involve sectioning. We propose that these actin-based protrusions are functionally required for efficient fusion, as such structures are disassembled in cells that just fused and are virtually absent in fusion-incompetent Srf mutant cells.

Our results show that the absence of Srf expression leads to the blockade of fusion and the disruption of actin cytoskeleton organization. The major changes in the actin scaffold observed in Srf mutant cell—including less total actin and F-actin, fewer actin cables in the ventral part of the cell, and the absence of protrusion—can be attributed to Mrtf/Srf signaling being a key mediator of the cytoskeletal response to Rho family GTPase activation and actin cycling in wild-type cells (Esnault et al., 2014). Indeed, we showed that in addition to genes encoding actins, several regulators of actin cytoskeleton organization are controlled by Srf (including *Abra*, *Cnn2*, *Fermt2*, *FlnA*, *Tgfb1i1*, and *Wdr1*), and they all have been identified as direct Srf targets (Wang et al., 2011; Chong et al., 2012; Esnault et al., 2014). Several of these targets could be implicated in the formation of the actin-based protrusions. For instance, Fermt2 adaptor protein has recently been shown to associate with the Arp2/3 complex and induce Rac1-mediated membrane protrusions in fibroblasts (Böttcher et al., 2017). In addition, the actin regulator filamin-A has been shown to modulate filopodia formation through Cdc42 GTPase activation in lung carcinoma and melanoma cell lines (Chiang et al., 2017). Of note, both Rac1 and Cdc42 have been genetically linked to fusion defects in mammals (Vasyutina et al., 2009).

Remarkably, the overexpression of α-cardiac actin alone in Srf mutant cells restored actin architecture and rescued heterotypic fusion between a control MB/MT and a mutant MB and overcame the need for Srf expression in both fusion partners for efficient fusion, both in vitro and in vivo. In other words, fusion can take place between a control cell and a Srf mutant cell if its F-actin content and the organization of actin into cables are recovered. The possible underlying mechanism for this rescue could be restoration of the mechanical invading force that helps to overcome energy barriers for membrane apposition and drives cell membrane fusion (Kim et al., 2015b) or the appropriate cellular distribution of signaling molecules or contractile protein molecules required for fusion (Tran et al., 2012; Simionescu-Bankston et al., 2015).

Our study also shows that maintenance of the actin network in Srf-depleted SCs, achieved by the sole overexpression of α-cardiac actin, was not sufficient for the in vitro and in vivo (during muscle regeneration) reestablishment of homotypic fusion between two Srf mutant cells, suggesting that additional Srf targets involved in other cellular processes are required. In *Drosophila*, the initial invasive activity provided by actin foci triggers a mechanosensitive

accumulation of myosin motors in the receiving cell to the site of invasion, which in turn generates cortical stiffness to facilitate fusion (Kim et al., 2015b). By controlling the expression of *Myl9* and *Myh9* (Medjkane et al., 2009), two components of the actomyosin network, Srf could contribute to the maintenance of mechanical tension/rigidity allowing, in concert with actin-based protrusions, productive invasion, and fusion.

The role of SCs in muscle hypertrophy as donors of new nuclei and contributors to muscle growth has been a highly debated issue (Pallafacchina et al., 2013; Blaauw and Reggiani, 2014; Snijders et al., 2015; Gundersen, 2016; Egner et al., 2017; McCarthy et al., 2017). Using a mouse model of SC ablation, McCarthy et al. (2011) showed that SCs were not required for plantaris muscle growth after overload. Egner et al. (2016) found that overload-induced hypertrophy was prevented in both SC-ablated plantaris and EDL muscles. A recent study suggested that this discrepancy may be attributed to the age of the mice, as young mice (<4 mo old) require SCs to undergo overload-induced myofiber hypertrophy, whereas mature mice (>4 mo old) do not require SCs but display an increased fiber number and size after CH (Murach et al., 2017). Our study (performed on 3-mo-old mice) provides new genetic evidence showing that hypertrophy is compromised when SCs are unable to fuse and is in agreement with the requirement of Myomaker, a known mammalian MB fusogen, in muscle hypertrophy (Goh and Millay, 2017). In vivo overexpression of α-actin in Srf mutant SCs rescued both fusion and overall growth in the overload-induced hypertrophy model, indicating the necessity of SC myonuclear accretion for optimal hypertrophic physiological muscle growth.

Collectively, our study reveals Srf as a key regulator of SC fusion and highlights the crucial role played by actin filaments to drive fusion in vitro and in vivo. Indeed, we report the existence of finger-like actin-based structures at the site of fusion only in fusion-competent mammalian cells. More generally, our data strongly support the requirement of SC-mediated fusion in myofiber hypertrophy.

Materials and methods

Mouse protocols

Srf$^{flox/flox}$ mice are homozygous for Srf floxed alleles harboring LoxP sites flanking exon 2 of endogenous *Srf* gene (Parlakian et al., 2004). *Pax7*$^{CreERT2/+}$ knock-in mice express Cre-ERT2 recombinase from the endogenous *Pax7* locus (provided by C.M. Fan, Carnegie Institution for Science, Washington, DC; Lepper et al., 2009), and Tg:*Pax7-nGFP* transgenic mice express nuclear localized EGFP under the Pax7 promoter (provided by S. Tajbakhsh, Pasteur Institute, Paris, France; BAC containing 55-kbp upstream Pax7 initiator ATG; Sambasivan et al., 2009).

To investigate the effect of SC-specific *Srf* deletion in adult muscle, the mouse strain *Pax7*$^{CreERT2/+}$*:Srf*$^{flox/flox}$*:Pax7-nGFP* was generated. In all experiments, 3-mo-old *Pax7*$^{CreERT2/+}$*:Srf*$^{flox/flox}$*:Pax7-nGFP* mice were given five i.p. injections of TMX (1 mg/d; MP Biomedicals) to induce *Srf* deletion and were referred to as mutant mice. Both *Pax7*$^{+/+}$*:Srf*$^{flox/flox}$*:Pax7-nGFP* mice injected with TMX and noninjected *Pax7*$^{CreERT2/+}$*:Srf*$^{flox/flox}$*:Pax7-nGFP* mice were initially used as control mice. However, because all muscle phenotypes investigated were identical between these two controls, uninjected *Pax7*$^{CreERT2/+}$*:Srf*$^{flox/flox}$*:Pax7-nGFP* mice were used as control mice (control) in the experiments here. No statistical differences in body weights were observed after TMX in *Pax7*$^{CreERT2/+}$*:Srf*$^{flox/flox}$*:Pax7-nGFP* mice.

To assay whether the overexpression of α-actin could rescue some of the outcomes of the *Srf* loss, we used a transgenic mouse model (*CMV-flx-CAT-flx-Actc1*) allowing the inducible and conditional overexpression of exogenous rat *α-cardiac actin* (*Actc1*) when bred with a Cre driver mouse line. The transgenic construction is composed of β-actin promoter and cytomegalovirus enhancer ensuring the transgene expression. The cDNA of the rat α-cardiac actin (Actc1) is downstream of the chloramphenicol acetyl transferase (CAT) gene flanked by loxP sites. Polyadenylation sites downstream of the CAT gene preclude the expression of α-cardiac actin. *CMV-flx-CAT-flx-Actc1* mice were bred with *Pax7*$^{CreERT2/+}$*:Srf*$^{flox/flox}$*:Pax7-nGFP* mice to obtain *Pax7*$^{CreERT2/+}$*:Srf*$^{flox/flox}$*:Pax7-nGFP:CMV-flx-CAT-flx-Actc1* mice, in which TMX injections permit *Srf* loss, the deletion of the CAT cassette, and the concomitant overexpression of *Actc1* in SCs. TMX-injected *Pax7*$^{CreERT2/+}$*:Srf*$^{flox/flox}$*:Pax7-nGFP:CMV-flx-CAT-flx-Actc1* were referred to as Mut/Act^{+} mice.

Mice were genotyped by PCR using the following primers: Gfp-F, 5′-CGACGTAAACGGCCACAAGTTC-3′; Gfp-R, 5′-GACGTTGTGGCTGTTGTAGTTG-3′; Cre-F, 5′-CCTGGAAAATGCTTCTGTCCG-3′; Cre-R, 5′-CAGGGTGTTATAAGCAATCCC-3′; ActTg-F, 5′-CGAGGGACCTAATAACTTCG-3′; ActTg-R, 5′-GCCGGATAAAACTTGTGCTT-3′; Srflox-F, 5′-TTCGGAACTGCCGGGCACTAAA-3′; and Srflox-R, 5′-CTGTAAGGGATGGAAGCAGA-3′.

CH of plantaris muscles of control, mutant, and Mut/Act^{+} mice was induced through the incapacitation of soleus and gastrocnemius muscles by sectioning their tendon, in both legs. During the process of CH, mutant and Mut/Act^{+} mice were injected with TMX on days 2 and 4 after CH. At the indicated time (1, 3, and 5 wk after CH), plantaris muscles were dissected and processed for histological analyses. When indicated, mice were administered 25 µg/g EdU (Life Technologies).

Muscle tissue injury in control, mutant, and Mut/Act^{+} mice was achieved by a single intramuscular injection of 30 µl of 6 µM CTX (Latoxan) into TA muscle. During the process of regeneration, mutant and Mut/Act^{+} mice were injected with TMX on days 2 and 4 after CTX. Mice were allowed to recover for 30 d, and TA muscles were harvested. All animal experiments were conducted in accordance with the European Guidelines for the Care and Use of Laboratory Animals and were approved by the institutional ethics committee (00315.1).

Single-fiber culture

Individual fibers were isolated from EDL muscles of 2-mo-old control mice. EDL muscles were dissected by handling tendons only. Muscles were digested for 50 min at 35°C in 2 mg/ml collagenase I (Life Technologies) in DMEM/F12. When fibers were loosened, they were liberated using heat-polished glass Pasteur pipettes and selected by viewing under the microscope, and digestion was stopped with 20% FCS. Myofibers and associated SCs were either fixed in 4% PFA immediately after their isolation (quiescent SCs) or kept as nonadherent cultures for 24 h in DMEM, 20% FCS, 10% horse serum, and 1% chicken embryo extract (activated SCs) before fixation in 4% PFA. Myofibers were the stained against Pax7 (1/50; sc-81648; Santa Cruz Biotechnology) and Srf (1/100; sc 13029; Santa Cruz Biotechnology) and with DAPI. At least 30 Pax7^{+} cells were counted per experiment and in each condition.

Primary muscle cell culture and adenoviral transduction

Primary cultures were derived from hindlimb muscles of control, mutant, and Mut/Act^{+} of 6- to 8-wk-old mice all harboring the Pax7-nGFP transgene that allowed prospective selection of SCs by FACS. The dissection of the muscles was performed with care to take off as much fat and connective tissue as possible. The muscles were minced in DMEM/F12 supplemented with 2% antibiotic/antimycotic (15240-062; Gibco) in a sterile Petri dish on ice. The minced muscles were digested three

times for 25 min at 37°C with 1 mg/ml collagenase D (Roche) and 0.1% Trypsin (15090-046; Gibco), and digestion was stopped by adding FCS (25% final). Cells were filtered through a 70-µm cell strainer and pelleted. Cells were then washed three times in DMEM/F12 and 2% antibiotic/antimycotic, resuspended in 1× PBS without Ca^{2+} and Mg^{2+}, 2% FCS, and 2% antibiotic/antimycotic, and finally filtered with a 40-µm cell strainer. Pax7/GFP-positive SCs were sorted on FACSAria III (BD) previously calibrated (fluorescence minus one and use of compensation beads) using the CYBIO Cochin Institute platform. Cells were collected in a FACS tube containing FCS and 2% antibiotic/antimycotic.

In standard conditions, MBs were grown in growth medium (DMEM/F12, 2% Ultroser G [PALL Life Sciences], and 20% FCS) on plastic dishes coated with 0.02% Gelatin. For differentiation, MBs were seeded in Matrigel-coated dishes and cultured in differentiation medium (DMEM/F12 and 2% horse serum).

To induce in culture the excision of the floxed *Srf* allele, $Srf^{flox/flox}$ MBs were transduced twice with adenoviruses Ad-GFP or Ad-CreGFP (100 MOI). 2 d after the first transduction, GFP^+ MBs were purified by cell sorting with BD FACSAria III.

Proliferation assays

To detect S-phase entry, control and mutant SCs were plated immediately after sorting, cultured for 5 d in growth medium, and pulsed with EdU (10 µM; Life Technologies) for 2 h before fixation with 4% PFA. EdU detection was performed using a Click-iT EdU Alexa Fluor 647 kit, according to the manufacturer's instructions (Life Technologies).

For cell cycle analysis, control and mutant MBs were collected, fixed in 70% cold ethanol, washed with PBS, and resuspended in the staining buffer containing 50 µg/ml propidium iodide and 100 µg/ml RNase (Invitrogen). Cell cycle profiles were acquired using a BD Accuri C6 cytometer (BD Biosciences) and processed with NovoExpress software (ACEA).

Western blot analysis

Cells were lysed directly in 1× Laemmli buffer, and proteins were separated through denaturing SDS-PAGE electrophoresis using Mini-Protean TGX precast gels (Bio-Rad) and transferred to PVDF membrane using the wet method (Bio-Rad). Membranes were blocked with 5% skim milk in TBS-1% Tween (TBST) for 1 h at RT and probed overnight at 4°C with primary antibodies in TBST and 5% BSA. The following antibodies were used: mouse anti-Srf (1/1,000; sc 13029; Santa Cruz Biotechnology), rabbit anti–pan actin (1/750; AAN01-A; Cytoskeleton), and mouse anti–α tubulin (1/4,000; T 6074; Sigma-Aldrich). After washing in TBST, membranes were hybridized with goat anti-mouse and goat anti-rabbit secondary antibodies coupled to HRP (1/10,000; 62-6520 and A27036; Thermo Fisher Scientific). Proteins were revealed using SuperSignal West Femto substrate (Thermo Fisher Scientific).

Quantification of F/G-actin ratio

The ratio of filamentous (F-) to globular (G-) actin was determined using the G-actin/F-actin in vivo assay kit (Cytoskeleton). In brief, MBs were harvested, and lysates were cleared by centrifugation at 500 *g* for 5 min. Supernatants were centrifuged at 100,000 *g* for 1 h at 37°C, which resulted in F-actin in the pellet and G-actin in the supernatant. The F-actin–containing pellet was resuspended and solubilized in F-actin depolymerization buffer at a volume equal to that of the G-actin–containing supernatant. Equivalent volumes of supernatant and pellet were resolved by SDS-PAGE and subjected to immunoblot analysis using an anti–pan-actin antibody (Cytoskeleton). The F/G-actin ratio was quantified using FusionCapt Advance software (Vilber Lourmat).

Cell migration assay

Migration of primary mouse muscle cells was quantified using time-lapse microscopy. MBs were seeded in gelatin-coated eight-well Ibidi plates and maintained in rich medium. The next day, cells were filmed using an inverted Axio Observer Z1 microscope (Zeiss) with a LCI PlN 10×/0.8 W DICII objective and an incubation chamber at 37°C and 5% CO_2. Live cells were monitored every 6 min for 6 h with bright-field and Metamorph 7.7.5 software. Cell velocities were calculated in micrometers per minute using ImageJ (National Institutes of Health) by tracking the paths of cells. At least 150 cells were tracked for each sample.

Live F-actin imaging

Control MBs were cultured in Matrigel-coated eight-well Ibidi plates. After 1 d of differentiation, they were stained with 75 nM SiR-Actin (Tebu-Bio) for 5 h before filming with an inverted Axio Observer Z1 microscope with a EC-PLAN NEOFLUAR 40×/0.75 objective and an incubation chamber at 37°C and 5% CO_2. Live cells were monitored every 10 min for 16 h with bright-field and Cy5 filter using Metamorph v.7.7.5.

Cell mixing fusion assays

To analyze heterotypic fusion between MBs, control or mutant MBs were loaded with 6 µM Orange Cell Tracker (Molecular Probes) for 30 min and co-cultured with control, mutant, or Mut/Act^+ MBs loaded with 6 µM Deep Red Cell Tracker (Molecular Probes) for 30 min in differentiation medium. For heterotypic fusion between MT control and MB, control MTs at day 2 of differentiation were loaded with Orange Cell Tracker and co-cultured with control, mutant, or Mut/Act^+ MBs loaded with Deep Red Cell Tracker. 2 d after cell mixing, fusion events were scored by counting the dual-labeled cells. The number of fusion events was normalized by the total number of nuclei for MB–MB fusion and the total number of cells for MT–MB fusion.

Muscle section and cell immunostaining

Plantaris and TA muscles were collected and snap-frozen in liquid nitrogen–cooled isopentane. 8-µm-thick muscle sections were fixed in 4% PFA for 8 min at RT and blocked overnight at 4°C in PBS 1×, 10% horse serum, and 0.5% Triton X-100, then incubated with primary antibodies overnight at 4°C in PBS 1×, 10% horse serum, and 0.5% Triton X-100. The following primary antibodies were used: mouse anti-dystrophin (1/50; NCL-Dys2; Novocastra), rabbit anti-laminin (L9393, 1/200; Sigma-Aldrich), and rabbit anti-myogenin (1/100; sc-576; Santa Cruz Biotechnology). After washes in PBS 1×, sections were incubated with secondary antibodies for 1 h at RT. The following secondary antibodies were used: goat anti–mouse IgG1 Alexa Fluor 488 (1/1,000; A21121; Thermo Fisher Scientific) and donkey anti-rabbit Alexa Fluor 546 (1/1,000; A10040; Life Technologies). Nucleus staining was performed using DAPI. Muscle sections were then mounted in Dako Fluorescence Mounting Medium and kept at 4°C until image acquisition.

For Pax7 staining, muscle sections were fixed in 4% PFA for 8 min at RT and permeabilized in ice-cold methanol for 6 min. Muscle sections were treated with Antigen Unmaking Solution, pH 6.0 (H-3300; Vector Laboratories) for 15 min at 95°C and cooled on ice for 30 min. Blocking and incubation with primary and secondary antibodies were conducted as described in the preceding paragraph. Primary mouse anti-Pax7 antibody (sc-81648; Santa Cruz Biotechnology) was used at dilution 1/50. EdU detection was performed using Click-iT EdU Alexa Fluor 647 kit, according to the manufacturer's instructions (Life Technologies).

Muscle cells cultured in dishes were fixed for 8 min in 4% PFA and then permeabilized and blocked in PBS with 0.1% Triton X-100 and 5% horse serum for 1 h at RT. Cells were incubated overnight at 4°C

with the following primary antibodies: mouse anti-MyoD (1/100; SC-760; Santa Cruz Biotechnology), rabbit anti-myogenin (1/100; sc-576; Santa Cruz Biotechnology), mouse anti-MHC embryonic (1/50; MF20; Alexis Biochemical), and rabbit anti–phospho histone H3 (1/500; 3377; Cell Signaling Technology) diluted in the same buffer. After incubation for 1 h at RT with fluorescent secondary antibodies anti–mouse IgG1 Alexa 488 (1/1,000; A21121) and donkey anti-rabbit Alexa Fluor 546 (1/1,000; A10040; Life Technologies), cells were stained with DAPI (for nuclei) and phalloidin Alexa Fluor 488 (1/500; Thermo Fisher Scientific; for F-actin) and mounted in Fluorescent Mounting Medium (Dako).

Morphometric analysis and phalloidin quantification

Myofiber CSA was analyzed by using immunostaining of dystrophin, marking myofiber sarcolemma, and then using ImageJ. 600–800 myofibers were analyzed. For the quantification of the number of nuclei per myofiber, at least 500 myofibers were counted. Phalloidin signal intensity per cell was quantified using ImageJ. At least 150 cells were analyzed.

Image acquisition

Digital images were acquired using an Olympus BX63F microscope with 10× objective (UplanFL, numerical aperture 0.3) and 20× objective (UPLSAPO, 0.75), ORCA-Flash4.0 LT C11440-42U camera (Hamamatsu); an Axiovert 200M microscope (Zeiss) with 5× objective (PLANFLUAR, 0.25) and 20× objective (LD PLANNEOFL UAR, 0.4), cooled CCD CoolSNAP-HQ^2 camera (Photometrics); or a Spinning Disk Leica confocal microscope with a 100× oil-immersion objective (HCX PL APO, 1.47), cooled CCD CoolSNAP-HQ^2 camera (Photometrics) and Metamorph v.7.7.5 (Molecular Devices). Images were composed and edited in ImageJ. Background was reduced using brightness and contrast adjustments applied to the whole image.

Electron microscopy of unroofed cells

Adherent adult SCs were either cultured exclusively in proliferation medium or switched to fusion medium for 24 h before they were disrupted by sonication as described previously (Heuser, 2000). Glutaraldehyde/PFA-fixed cell cortices were further sequentially treated with OsO_4, tannic acid, and uranyl acetate before dehydration and hexamethyldisilazane drying (Sigma-Aldrich). Dried samples were then rotary-shadowed with platinum and carbon with a high vacuum metal coater (Leica). Platinum replicas were floated off the glass by flotation on hydrofluoric acid, washed several times in distilled water, and picked up on formvar/carbon-coated electromagnetic grids. The grids were mounted in a eucentric side-entry goniometer stage of a transmission electron microscope operated at 80 kV (model CM120; Philips), and images were recorded with a Morada digital camera (Olympus). Images were processed in Adobe Photoshop to adjust brightness and contrast and presented in inverted contrast. Anaglyphs were made by converting the −10° tilt image to red and the 10° tilt image to cyan (blue/green), layering them on top of each other using the screen blending mode in Adobe Photoshop, and aligning them to each other.

RNA extraction and quantitative real-time (qRT)–PCR

RNA extraction and qRT-PCR analysis were performed as described previously (Guerci et al., 2012). Values were normalized using *Hydroxymethylbilane synthetase* (*Hmbs*). The following primers were used: Srf-F, 5′-CACCTACCAGGTGTCGGAAT-3′; Srf-R, 5′-GCTGTGTGGATTGTGGAGGT-3′; MyoD-F, 5′-GCAGATGCACCACCAGAGTC-3′; MyoD-R, 5′-TTCCTGGG-TCCAGCCTCAAC-3′; Myogenin-F, 5′-GCAATGCACTGGAGTTCG-3′; Myogenin-R, 5′-ACGATGGACGTAAGG-GAGTG-3′; Acta1-F, 5′-CTGAGCGCAAGTACTCAGTGT-GGA-3′; Acta1-R, 5′-TTCCAA-AAACAGGCGCCGGCTGCA-3′; Acta2-F, 5′-GTCC-CAGACATCAGGGAGTAA-3′; Acta2-R, 5′-TCGGATACTTCAGCGTCAGGA-3′; Actc1-F, 5′-ACTCTCTTCCAGCCCTCTTTCATT-3′; Actc1-R 5′-GAGCCAGTGCAGTG-ATTTCCTT-3′; Actb-F, 5′-GTGGCATCCATGAA-ACTACAT-3′; Actb-R, 5′-GGCATAGAGGTCTTTACGG-3′; Actg-F, 5′-GGCTTACACTGCGCTTCTTG-3′; Actg-R, 5′-GAGTGCGGCGATTTCTTCTT-3′; ActTg-F, 5′-TGCTGGTTATTGTGCTGTCT-3′; ActTg-R, 5′-CTGTGGTCTCCTCGTCGT-3′; Abra-F, 5′-ATCGAGACGGAGAGGGACAA-3′; Abra-R, 5′-TTGCTGACAACCGTTCTGGT-3′; Cnn2-F, 5′-AATGGGCTTCCTG-TTTCTTCATCT-3′; Cnn2-R, 5′-TCGTGGGAAAGCAAA-CTTAGTCC-3′; Fermt2-F, 5′-AGTGGAATGTCAACTGGGAGATC-3′; Fermt2-R, 5′-GGACAACCGGACCT-CATCTG-3′; Flna-F, 5′-GATTGGGGAGGAGACGGTGAT-3′; Flna-R, 5′-TTTGCT-GGCTACCCTGAGGATAG-3′; Tgfb1i1-F, 5′-GCCTCTGTGGCTCCTG-CAATAAAC-3′; Tgfb1i1-R, 5′-CTTCTCGAAGAAGCTGCTGCCTC-3′; Wdr1-F, 5′-TGGAGCGG-GGCGTCTCTA-3′; Wdr1-R, 5′-AATCCGCTGGGTGCATACTTG-3′; Hmbs-F, 5′-TGCACGATCCTGAAACTCTG-3′; and Hmbs-R, 5′-TGCATGCTATCTGAGCCATC-3′.

Affymetrix microarrays

Microarray analysis was performed from three independent Ad-GFP– and Ad-CreGFP–transduced cell cultures. Total RNAs were obtained from cells at day 0 (corresponding to MBs), day 1 (corresponding to myocytes), and day 3 (corresponding to MTs) of differentiation, using RNeasy Mini kit (Qiagen) and DNase treatment (Qiagen). RNA integrity was certified on a bioanalyzer (Agilent). Hybridization to Mouse Gene 2.0-ST arrays (Affymetrix) and scans (GCS3000 7G Expression Console software) were performed on the Genom'ic platform (Institut Cochin, Paris, France). Probe data normalization and gene expression levels were processed using the robust multiarray average (RMA) algorithm in expression Console (Affymetrix). Gene ontology analysis was performed using Ingenuity (IPA) software. Full data are available on Gene Expression Omnibus: GSE105125.

Statistical analysis

Quantitative datasets were analyzed using unpaired nonparametric Mann–Whitney test (Fig. 2, C and D; Fig. 3 E; Fig. 4, C, D, and F; and Fig. S1, C–E), unpaired *t* test (Figs. 2 E and S1 H), one-way ANOVA with Bonferroni's multiple comparisons test (Fig. 4 E; Fig. 6, B, D, and F; Fig. 8, B–D and F; and Fig. S4, C and F), or two-way ANOVA with Bonferroni's multiple comparisons test (all other datasets) using GraphPad Prism 6 software. Statistical significance was set at $P < 0.05$.

Online supplemental material

Fig. S1 describes the validation of the genetic model used and the efficient loss of Srf in SCs. In addition, the phenotype of Srf-deleted SC (unaffected proliferation and differentiation and impaired motility) was confirmed by deleting Srf ex vivo using Ad-Cre transduction of Srfflox/flox MBs. Fig. S2 illustrates an alternative method to monitor the fusion defect of Srf mutant SCs in vivo. In search for the genes whose altered expression could participate in Srf mutant SC fusion defect, we quantified the expression of several genes encoding actin isoforms and regulators of actin cytoskeleton in a model of ex vivo Srf deletion (Ad-Cre transduction of Srfflox/flox MBs). Fig. S3, Video 1 (bright field), and Video 2 (Sir-Actin) show F-actin reorganization upon fusion by F-actin live imaging. Additional EM images of unroofed cells are represented. Fig. S4 describes the genetic model allowing the concomitant loss of Srf and Actc1 overexpression in SCs and the impact of Actc1 overexpression on Srf mutant MB motility and differentiation. Fig. S5 depicts the regeneration process (myofiber number and SC number) in Srf mutant muscles. Table S1 is a list of the genes whose expressions in muscle cells depend on Srf.

Acknowledgments

We thank CM. Fan (Carnegie Institution for Science, Washington, DC) and S. Tajbakhsh (Pasteur Institute, Paris, France) for providing *Pax-7*$^{CreERT2/+}$ and *Pax7-nGFP* mice, respectively. We acknowledge the CYBIO, IMAG'IC, Genom'IC, and Animal Care core facilities of Cochin Institute as well as the Institut de Biologie Paris-Seine EM platform. We are grateful to S. Colnot for critical reading of the manuscript and to T. Guilbert for assistance in the video presentations (Cochin Institute, Paris, France).

This work was supported by grants from Association Française contre les Myopathies (20975 to A. Sotiropoulos and A. Papaefthymiou), Labex WhoAmI? (to A. Sotiropoulos and A. Pincini), Idex Sorbonne Paris Cité (to A. Sotiropoulos and U. Faradova), and Agence Nationale de la Recherche (ANR-13-BSV1-MECHANO to A. Sotiropoulos and ANR-14-CE12-0001-01 to S. Vassilopoulos).

The authors declare no competing financial interests.

Author contributions: V. Randrianarison-Huetz, A. Papaefthymiou, and S. Vassilopoulos designed and carried out experiments, analyzed results, and wrote the manuscript. G. Herledan, C. Noviello, U. Faradova, L. Collard, A. Pincini, and E. Schol conducted experiments and analyzed results. J.F. Decaux and P. Maire provided reagents and expertise. A. Sotiropoulos designed and carried out experiments, analyzed results, wrote the manuscript, and provided financial support.

Submitted: 22 May 2017
Revised: 20 October 2017
Accepted: 21 November 2017

References

Almada, A.E., and A.J. Wagers. 2016. Molecular circuitry of stem cell fate in skeletal muscle regeneration, ageing and disease. *Nat. Rev. Mol. Cell Biol.* 17:267–279. https://doi.org/10.1038/nrm.2016.7

Blaauw, B., and C. Reggiani. 2014. The role of satellite cells in muscle hypertrophy. *J. Muscle Res. Cell Motil.* 35:3–10. https://doi.org/10.1007/s10974-014-9376-y

Böttcher, R.T., M. Veelders, P. Rombaut, J. Faix, M. Theodosiou, T.E. Stradal, K. Rottner, R. Zent, F. Herzog, and R. Fässler. 2017. Kindlin-2 recruits paxillin and Arp2/3 to promote membrane protrusions during initial cell spreading. *J. Cell Biol.* 216:3785–3798. https://doi.org/10.1083/jcb.201701176

Carnac, G., M. Primig, M. Kitzmann, P. Chafey, D. Tuil, N. Lamb, and A. Fernandez. 1998. RhoA GTPase and serum response factor control selectively the expression of MyoD without affecting Myf5 in mouse myoblasts. *Mol. Biol. Cell.* 9:1891–1902. https://doi.org/10.1091/mbc.9.7.1891

Cenik, B.K., N. Liu, B. Chen, S. Bezprozvannaya, E.N. Olson, and R. Bassel-Duby. 2016. Myocardin-related transcription factors are required for skeletal muscle development. *Development.* 143:2853–2861. https://doi.org/10.1242/dev.135855

Charvet, C., C. Houbron, A. Parlakian, J. Giordani, C. Lahoute, A. Bertrand, A. Sotiropoulos, L. Renou, A. Schmitt, J. Melki, et al. 2006. New role for serum response factor in postnatal skeletal muscle growth and regeneration via the interleukin 4 and insulin-like growth factor 1 pathways. *Mol. Cell. Biol.* 26:6664–6674. https://doi.org/10.1128/MCB.00138-06

Chiang, T.S., H.F. Wu, and F.J. Lee. 2017. ADP-ribosylation factor-like 4C binding to filamin-a modulates filopodium formation and cell migration. Mol. Biol. Cell.28:3013–3028.

Chong, N.W., A.L. Koekemoer, S. Ounzain, N.J. Samani, J.T. Shin, and S.Y. Shaw. 2012. STARS is essential to maintain cardiac development and function in vivo via a SRF pathway. *PLoS One.* 7:e40966. https://doi.org/10.1371/journal.pone.0040966

Collard, L., G. Herledan, A. Pincini, A. Guerci, V. Randrianarison-Huetz, and A. Sotiropoulos. 2014. Nuclear actin and myocardin-related transcription factors control disuse muscle atrophy through regulation of Srf activity. *J. Cell Sci.* 127:5157–5163. https://doi.org/10.1242/jcs.155911

Dhanyasi, N., D. Segal, E. Shimoni, V. Shinder, B.Z. Shilo, K. VijayRaghavan, and E.D. Schejter. 2015. Surface apposition and multiple cell contacts promote myoblast fusion in *Drosophila* flight muscles. *J. Cell Biol.* 211:191–203. https://doi.org/10.1083/jcb.201503005

Dumont, N.A., Y.X. Wang, and M.A. Rudnicki. 2015. Intrinsic and extrinsic mechanisms regulating satellite cell function. *Development.* 142:1572–1581. https://doi.org/10.1242/dev.114223

Egner, I.M., J.C. Bruusgaard, and K. Gundersen. 2016. Satellite cell depletion prevents fiber hypertrophy in skeletal muscle. *Development.* 143:2898–2906. https://doi.org/10.1242/dev.134411

Egner, I.M., J.C. Bruusgaard, and K. Gundersen. 2017. An apparent lack of effect of satellite cell depletion on hypertrophy could be due to methodological limitations. Response to 'Methodological issues limit interpretation of negative effects of satellite cell depletion on adult muscle hypertrophy'. *Development.* 144:1365–1367. https://doi.org/10.1242/dev.148163

Esnault, C., A. Stewart, F. Gualdrini, P. East, S. Horswell, N. Matthews, and R. Treisman. 2014. Rho-actin signaling to the MRTF coactivators dominates the immediate transcriptional response to serum in fibroblasts. *Genes Dev.* 28:943–958. https://doi.org/10.1101/gad.239327.114

Gauthier-Rouviere, C., M. Vandromme, D. Tuil, N. Lautredou, M. Morris, M. Soulez, A. Kahn, A. Fernandez, and N. Lamb. 1996. Expression and activity of serum response factor is required for expression of the muscle-determining factor MyoD in both dividing and differentiating mouse C2C12 myoblasts. *Mol. Biol. Cell.* 7:719–729. https://doi.org/10.1091/mbc.7.5.719

Goh, Q., and D.P. Millay. 2017. Requirement of myomaker-mediated stem cell fusion for skeletal muscle hypertrophy. *eLife.* 6:e20007. https://doi.org/10.7554/eLife.20007

Gruenbaum-Cohen, Y., I. Harel, K.B. Umansky, E. Tzahor, S.B. Snapper, B.Z. Shilo, and E.D. Schejter. 2012. The actin regulator N-WASp is required for muscle-cell fusion in mice. *Proc. Natl. Acad. Sci. USA.* 109:11211–11216. https://doi.org/10.1073/pnas.1116065109

Gualdrini, F., C. Esnault, S. Horswell, A. Stewart, N. Matthews, and R. Treisman. 2016. SRF co-factors control the balance between cell proliferation and contractility. *Mol. Cell.* 64:1048–1061. https://doi.org/10.1016/j.molcel.2016.10.016

Guerci, A., C. Lahoute, S. Hébrard, L. Collard, D. Graindorge, M. Favier, N. Cagnard, S. Batonnet-Pichon, G. Précigout, L. Garcia, et al. 2012. Srf-dependent paracrine signals produced by myofibers control satellite cell-mediated skeletal muscle hypertrophy. *Cell Metab.* 15:25–37. https://doi.org/10.1016/j.cmet.2011.12.001

Gundersen, K. 2016. Muscle memory and a new cellular model for muscle atrophy and hypertrophy. *J. Exp. Biol.* 219:235–242. https://doi.org/10.1242/jeb.124495

Heuser, J. 2000. The production of 'cell cortices' for light and electron microscopy. *Traffic.* 1:545–552. https://doi.org/10.1034/j.1600-0854.2000.010704.x

Hindi, S.M., M.M. Tajrishi, and A. Kumar. 2013. Signaling mechanisms in mammalian myoblast fusion. *Sci. Signal.* 6:re2. https://doi.org/10.1126/scisignal.2003832

Kalo, A., I. Kanter, A. Shraga, J. Sheinberger, H. Tzemach, N. Kinor, R.H. Singer, T. Lionnet, and Y. Shav-Tal. 2015. Cellular levels of signaling factors are sensed by β-actin alleles to modulate transcriptional pulse intensity. *Cell Reports.* 11:419–432. https://doi.org/10.1016/j.celrep.2015.03.039

Kim, J.H., P. Jin, R. Duan, and E.H. Chen. 2015a. Mechanisms of myoblast fusion during muscle development. *Curr. Opin. Genet. Dev.* 32:162–170. https://doi.org/10.1016/j.gde.2015.03.006

Kim, J.H., Y. Ren, W.P. Ng, S. Li, S. Son, Y.S. Kee, S. Zhang, G. Zhang, D.A. Fletcher, D.N. Robinson, and E.H. Chen. 2015b. Mechanical tension drives cell membrane fusion. *Dev. Cell.* 32:561–573. https://doi.org/10.1016/j.devcel.2015.01.005

L'honore, A., N.J. Lamb, M. Vandromme, P. Turowski, G. Carnac, and A. Fernandez. 2003. MyoD distal regulatory region contains an SRF binding CArG element required for MyoD expression in skeletal myoblasts and during muscle regeneration. *Mol. Biol. Cell.* 14:2151–2162. https://doi.org/10.1091/mbc.E02-07-0451

Lepper, C., S.J. Conway, and C.M. Fan. 2009. Adult satellite cells and embryonic muscle progenitors have distinct genetic requirements. *Nature.* 460:627–631. https://doi.org/10.1038/nature08209

Li, S., M.P. Czubryt, J. McAnally, R. Bassel-Duby, J.A. Richardson, F.F. Wiebel, A. Nordheim, and E.N. Olson. 2005. Requirement for serum response factor for skeletal muscle growth and maturation revealed by tissue-specific gene deletion in mice. *Proc. Natl. Acad. Sci. USA.* 102:1082–1087. https://doi.org/10.1073/pnas.0409103102

Martin, S.G. 2016. Role and organization of the actin cytoskeleton during cell-cell fusion. *Semin. Cell Dev. Biol.* 60:121–126. https://doi.org/10.1016/j.semcdb.2016.07.025

McCarthy, J.J., J. Mula, M. Miyazaki, R. Erfani, K. Garrison, A.B. Farooqui, R. Srikuea, B.A. Lawson, B. Grimes, C. Keller, et al. 2011. Effective fiber hypertrophy in satellite cell-depleted skeletal muscle. *Development.* 138:3657–3666. https://doi.org/10.1242/dev.068858

McCarthy, J.J., E.E. Dupont-Versteegden, C.S. Fry, K.A. Murach, and C.A. Peterson. 2017. Methodological issues limit interpretation of negative effects of satellite cell depletion on adult muscle hypertrophy. *Development.* 144:1363–1365. https://doi.org/10.1242/dev.145797

Medjkane, S., C. Perez-Sanchez, C. Gaggioli, E. Sahai, and R. Treisman. 2009. Myocardin-related transcription factors and SRF are required for cytoskeletal dynamics and experimental metastasis. *Nat. Cell Biol.* 11:257–268. https://doi.org/10.1038/ncb1833

Mokalled, M.H., A.N. Johnson, E.E. Creemers, and E.N. Olson. 2012. MAS TR directs MyoD-dependent satellite cell differentiation during skeletal muscle regeneration. *Genes Dev.* 26:190–202. https://doi.org/10.1101/gad.179663.111

Murach, K.A., S.H. White, Y. Wen, A. Ho, E.E. Dupont-Versteegden, J.J. McCarthy, and C.A. Peterson. 2017. Differential requirement for satellite cells during overload-induced muscle hypertrophy in growing versus mature mice. *Skelet. Muscle.* 7:14. https://doi.org/10.1186/s13395-017-0132-z

Nordheim, A. 2014. SRF regulation—Actin branches out. *Nat. Rev. Mol. Cell Biol.* 15:368. https://doi.org/10.1038/nrm3803

Nowak, K.J., G. Ravenscroft, C. Jackaman, A. Filipovska, S.M. Davies, E.M. Lim, S.E. Squire, A.C. Potter, E. Baker, S. Clément, et al. 2009. Rescue of skeletal muscle α-actin–null mice by cardiac (fetal) α-actin. *J. Cell Biol.* 185:903–915. https://doi.org/10.1083/jcb.200812132

Pallafacchina, G., B. Blaauw, and S. Schiaffino. 2013. Role of satellite cells in muscle growth and maintenance of muscle mass. *Nutr. Metab. Cardiovasc. Dis.* 23(Suppl 1):S12–S18. https://doi.org/10.1016/j.numecd.2012.02.002

Parlakian, A., D. Tuil, G. Hamard, G. Tavernier, D. Hentzen, J.P. Concordet, D. Paulin, Z. Li, and D. Daegelen. 2004. Targeted inactivation of serum response factor in the developing heart results in myocardial defects and embryonic lethality. *Mol. Cell. Biol.* 24:5281–5289. https://doi.org/10.1128/MCB.24.12.5281-5289.2004

Pipes, G.C., E.E. Creemers, and E.N. Olson. 2006. The myocardin family of transcriptional coactivators: Versatile regulators of cell growth, migration, and myogenesis. *Genes Dev.* 20:1545–1556. https://doi.org/10.1101/gad.1428006

Posern, G., and R. Treisman. 2006. Actin' together: Serum response factor, its cofactors and the link to signal transduction. *Trends Cell Biol.* 16:588–596. https://doi.org/10.1016/j.tcb.2006.09.008

Sambasivan, R., B. Gayraud-Morel, G. Dumas, C. Cimper, S. Paisant, R.G. Kelly, and S. Tajbakhsh. 2009. Distinct regulatory cascades govern extraocular and pharyngeal arch muscle progenitor cell fates. *Dev. Cell.* 16:810–821. https://doi.org/10.1016/j.devcel.2009.05.008

Schejter, E.D. 2016. Myoblast fusion: Experimental systems and cellular mechanisms. *Semin. Cell Dev. Biol.* 60:112–120. https://doi.org/10.1016/j.semcdb.2016.07.016

Segal, D., N. Dhanyasi, E.D. Schejter, and B.Z. Shilo. 2016. Adhesion and fusion of muscle cells are promoted by filopodia. *Dev. Cell.* 38:291–304. https://doi.org/10.1016/j.devcel.2016.07.010

Sens, K.L., S. Zhang, P. Jin, R. Duan, G. Zhang, F. Luo, L. Parachini, and E.H. Chen. 2010. An invasive podosome-like structure promotes fusion pore formation during myoblast fusion. *J. Cell Biol.* 191:1013–1027. https://doi.org/10.1083/jcb.201006006

Shin, N.Y., H. Choi, L. Neff, Y. Wu, H. Saito, S.M. Ferguson, P. De Camilli, and R. Baron. 2014. Dynamin and endocytosis are required for the fusion of osteoclasts and myoblasts. *J. Cell Biol.* 207:73–89. https://doi.org/10.1083/jcb.201401137

Simionescu-Bankston, A., C. Pichavant, J.P. Canner, L.H. Apponi, Y. Wang, C. Steeds, J.T. Olthoff, J.J. Belanto, J.M. Ervasti, and G.K. Pavlath. 2015. Creatine kinase B is necessary to limit myoblast fusion during myogenesis. *Am. J. Physiol. Cell Physiol.* 308:C919–C931. https://doi.org/10.1152/ajpcell.00029.2015

Snijders, T., J.P. Nederveen, B.R. McKay, S. Joanisse, L.B. Verdijk, L.J. van Loon, and G. Parise. 2015. Satellite cells in human skeletal muscle plasticity. *Front. Physiol.* 6:283. https://doi.org/10.3389/fphys.2015.00283

Soulez, M., C.G. Rouviere, P. Chafey, D. Hentzen, M. Vandromme, N. Lautredou, N. Lamb, A. Kahn, and D. Tuil. 1996. Growth and differentiation of C2 myogenic cells are dependent on serum response factor. *Mol. Cell. Biol.* 16:6065–6074. https://doi.org/10.1128/MCB.16.11.6065

Tran, T.H., X. Shi, J. Zaia, and X. Ai. 2012. Heparan sulfate 6-*O*-endosulfatases (Sulfs) coordinate the Wnt signaling pathways to regulate myoblast fusion during skeletal muscle regeneration. *J. Biol. Chem.* 287:32651–32664. https://doi.org/10.1074/jbc.M112.353243

Vandromme, M., C. Gauthier-Rouvière, G. Carnac, N. Lamb, and A. Fernandez. 1992. Serum response factor p67SRF is expressed and required during myogenic differentiation of both mouse C2 and rat L6 muscle cell lines. *J. Cell Biol.* 118:1489–1500. https://doi.org/10.1083/jcb.118.6.1489

Vasyutina, E., B. Martarelli, C. Brakebusch, H. Wende, and C. Birchmeier. 2009. The small G-proteins Rac1 and Cdc42 are essential for myoblast fusion in the mouse. *Proc. Natl. Acad. Sci. USA.* 106:8935–8940. https://doi.org/10.1073/pnas.0902501106

Wang, X., G. Hu, C. Betts, E.Y. Harmon, R.S. Keller, L. Van De Water, and J. Zhou. 2011. Transforming growth factor-β1-induced transcript 1 protein, a novel marker for smooth muscle contractile phenotype, is regulated by serum response factor/myocardin protein. *J. Biol. Chem.* 286:41589–41599. https://doi.org/10.1074/jbc.M111.250878